Developmental Biology **212,** 101–123 (1999)
Article ID dbio.1999.9356, available online at http://www.idealibrary.com on IDEAL®

Ultrastructural Features of the Adult Hermaphrodite Gonad of *Caenorhabditis elegans:* Relations between the Germ Line and Soma

David H. Hall,* Virginia P. Winfrey,† Gareth Blaeuer,† Loren H. Hoffman,†,[1] Tokiko Furuta,† Kimberly L. Rose,† Oliver Hobert,‡,[2] and David Greenstein†,[3]

**Center for C. elegans Anatomy, Department of Neuroscience, Albert Einstein College of Medicine, 1410 Pelham Parkway, Bronx, New York 10461; †Department of Cell Biology, Vanderbilt University School of Medicine, 21st and Garland, Nashville, Tennessee 37232-2175; and ‡Department of Molecular Biology, Massachussetts General Hospital, Boston, Massachusetts 02114*

Genetic and embryological experiments have established the *Caenorhabditis elegans* adult hermaphrodite gonad as a paradigm for studying the control of germline development and the role of soma–germline interactions. We describe ultrastructural features relating to essential germline events and the soma–germline interactions upon which they depend, as revealed by electron and fluorescence microscopy. Gap junctions were observed between oocytes and proximal gonadal sheath cells that contract to ovulate the oocyte. These gap junctions must be evanescent since individual oocytes lose contact with sheath cells when they are ovulated. In addition, proximal sheath cells are coupled to each other by gap junctions. Within proximal sheath cells, actin/myosin bundles are anchored to the plasma membrane at plaque-like structures we have termed hemi-adherens junctions, which in turn are closely associated with the gonadal basal lamina. Gap junctions and hemi-adherens junctions are likely to function in the coordinated series of contractions required to ovulate the mature oocyte. Proximal sheath cells are fenestrated with multiple small pores forming conduits from the gonadal basal lamina to the surface of the oocyte, passing through the sheath cell. In most instances where pores occur, extracellular yolk particles penetrate the gonadal basal lamina to directly touch the underlying oocytes. Membrane-bounded yolk granules were generally not found in the sheath cytoplasm by either electron microscopy or fluorescence microscopy. Electron microscopic immunocytochemistry was used to confirm and characterize the appearance of yolk protein in cytoplasmic organelles within the oocyte and in free particles in the pseudocoelom. The primary route of yolk transport apparently proceeds from the intestine into the pseudocoelom, then through sheath pores to the surface of the oocyte, where endocytosis occurs. Scanning electron microscopy was used to directly visualize the distal tip cell which extends tentacle-like processes that directly contact distal germ cells. These distal tip cell processes are likely to play a critical role in promoting germline mitosis. Scanning electron microscopy also revealed thin filopodia extending from the distal sheath cells. Distal sheath filopodia were also visualized using a green fluorescent protein reporter gene fusion and confocal microscopy. Distal sheath filopodia may function to stretch the sheath over the distal arm.

Key Words: **electron microscopy; germ line; oocyte; meiosis; gap junction; cell–cell interaction; *Caenorhabditis elegans*.**

INTRODUCTION

The formation of functional gametes is a complex and highly regulated developmental process that begins in the embryo and extends into the adult or sexually mature stage. In many organisms, germline precursor cells are set aside during early embryogenesis, migrate to colonize the gonad, and proliferate to generate a pool of germ cells for gametogenesis. During these events, the required mitotic and meiotic cell cycle transitions must be precisely coordinated with gametogenesis so that fertilization ultimately produces a diploid zygote capable of completing embryogenesis and growing into a fertile adult. Studies from a number of systems have shown that soma–germ cell interactions play critical roles in both the development of the germ line and the physiological functions of the sexually mature gonad. In

[1] Deceased.

[2] Present address: Department of Biochemistry and Molecular Biophysics, Columbia University, College of Physicians and Surgeons, New York, NY 10032.

[3] To whom correspondence should be addressed at Department of Cell Biology, Vanderbilt University School of Medicine, U-2224 MCN, 21st and Garland, Nashville, TN 37232-2175. Fax: 615-343-4539. E-mail: david.greenstein@mcmail.vanderbilt.edu.

0012-1606/99 $30.00

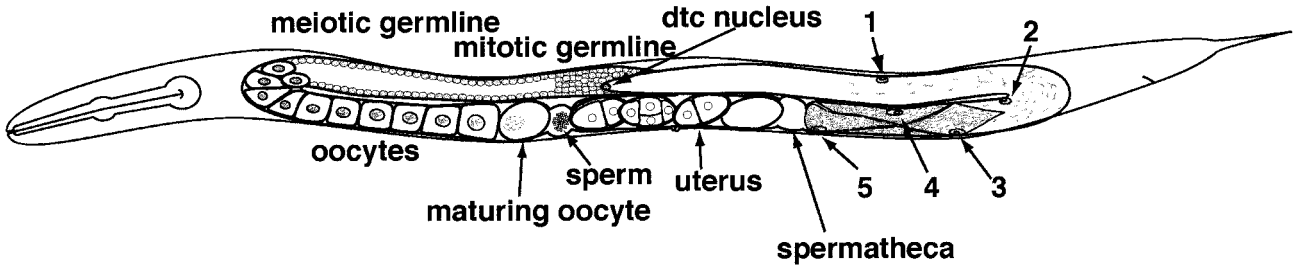

FIG. 1. Schematic representation of the adult hermaphrodite gonad (for review see Schedl, 1997). The anterior gonad arm (at left) depicts the germ line. Mitotic germ cells are located near the distal tip of the gonad arm. Meiotic germ cell nuclei extend to the loop region. Oocytes cellularize and grow in the proximal arm. The actual position where oocytes begin cellularization is age dependent. Oocytes remain in diakinesis prior to undergoing meiotic maturation in the most proximal position. Nuclear envelope breakdown of the maturing oocyte is represented by dotted lines. The posterior gonad arm (at right) depicts the somatic cells of the gonad arm. The position of one of each pair of sheath nuclei is indicated (Kimble and Hirsh, 1979). Sheath cells 3–5 of the proximal arm are visibly contractile and contain thick and thin filaments (indicated by stippling). Sheath cells 1 and 2 are not visibly contractile and cover part of the distal arm and the loop region, respectively.

the mouse, for example, Steel factor is expressed by cells in the gonadal ridges and along the primordial germ cell migratory pathway (Matsui *et al.*, 1990; Keshet *et al.*, 1991). Steel factor interacts with the c-kit receptor on germ cells and this interaction is required for germ cell proliferation, migration, and survival (for review, see Fleishman, 1993). Cell culture studies have indicated that c-kit signaling increases germ cell survival and promotes adhesion to somatic gonadal cells (Dolci *et al.*, 1991, 1993; Marziali *et al.*, 1993; Pesce *et al.*, 1997). While receptor–ligand interactions provide one mechanism for soma–germline interactions, gap junctions provide another. In the mammalian ovary, granulosa cells form gap junctions with oocytes (Anderson and Albertini, 1976). Mutational analysis suggests that intercellular signaling through these gap junctional channels is critical for oogenesis and ovulation (Simon *et al.*, 1997).

The nematode *Caenorhabditis elegans* provides an excellent model system for studying the control of germline development, gametogenesis, and the role of soma–germline interactions. The somatic gonad develops from a reproducible and largely invariant cell lineage, which has enabled the identification of soma–germline interactions using laser ablation (Kimble and White, 1981; McCarter *et al.*, 1997). Mutations affecting germline development and fertility have been obtained (for review see L'Hernault, 1997; and Schedl, 1997). The *C. elegans* adult hermaphrodite gonad consists of two equivalent U-shaped gonad arms (see Fig. 1) (Hirsh *et al.*, 1976; for review see Schedl, 1997). The distal portion of each gonad arm contains syncytial germline nuclei surrounded by incomplete membranes (Hirsh *et al.*, 1976). Although technically a syncytium, each germline nucleus and its associated cytoplasm are referred to as a germ cell. Mitotic germline nuclei are found within approximately 24 nuclear diameters from a specialized somatic cell, the distal tip cell, that determines the axial polarity of the gonad (Kimble and White, 1981). The distal tip cell maintains a mitotic germ cell population by virtue of an inductive cell interaction mediated by the GLP-1 signaling pathway (Hirsh *et al.*, 1976; Kimble and White, 1981; Austin and Kimble, 1987; Lambie and Kimble, 1991; Crittenden *et al.*, 1994; Berry *et al.*, 1997). As germline nuclei progress more proximally, away from the distal tip cell, they exit the mitotic cell cycle and enter meiosis. Cytologically recognizable nuclei in the pachytene stage of meiotic prophase I are visible before the "loop" (the U-shaped bend in the gonad arm; Hirsh *et al.*, 1976). Genetic and laser ablation studies have suggested that the exit of germ cells from the pachytene stage requires intercellular signaling (Church *et al.*, 1995; McCarter *et al.*, 1997). Germline nuclei undergo complete cellularization within the proximal gonad and differentiate as spermatocytes which complete meiosis to form approximately 160 sperm during the fourth larval stage of development (Hirsh *et al.*, 1976; Ward and Carrel, 1979). By contrast, upon progression to the adult stage, the germ cells differentiate as oocytes instead of sperm (Hirsh *et al.*, 1976), and they remain in the diakinesis stage of prophase I prior to undergoing meiotic maturation, ovulation, and fertilization (Ward and Carrel, 1979; McCarter *et al.*, 1997; Rose *et al.*, 1997). The meiotic maturation divisions of the oocyte are completed in the uterus (McCarter *et al.*, 1999), and embryogenesis begins.

We have analyzed the ultrastructure of the *C. elegans* adult hermaphrodite gonad employing electron and fluorescence microscopy. This analysis has revealed several ultrastructural features that were not reported by earlier microscopic investigations (Abi-Rached and Brun, 1975; Hirsh *et al.*, 1976; Strome 1986; White, 1988; Newman *et al.*, 1996) including sheath/oocyte gap junctions, sheath/sheath gap junctions, sheath pores, hemi-adherens junctions, and distal sheath filopodia. These structural features are likely to underlie soma–germline intercellular signaling and the reproductive functions of the adult gonad. These studies will form the basis for mutational analyses which will

ultimately be required to establish biological functions for these ultrastructural features.

MATERIALS AND METHODS

Transmission Electron Microscopy (TEM)

TEM on dissected gonadal preparations was performed as described (Rose *et al.*, 1997). L4 hermaphrodites were selected and cultured overnight (12–16 h) to the adult stage prior to dissection. The dissection procedure utilized serves to release the gonad from the body of the animal without altering its integrity or structure (Kimble and Sharrock, 1983; Francis *et al.*, 1995). Wild-type gonads (*C. elegans var* Bristol, strain N2 from the *Caenorhabditis* Genetics Center) were analyzed.

Intact wild-type adults were fixed for TEM in buffered aldehydes, postfixed in osmium tetroxide, and embedded in resin for serial sectioning according to standard methods (Hall, 1995). Animals were sectioned in either transverse or longitudinal thin sections, counterstained with uranyl acetate and/or lead citrate, and observed in a Philips CM10 or Hitachi H-800 electron microscope.

Freeze-Fracture Electron Microscopy

Wild-type adults were fixed in buffered 2.5% glutaraldehyde for 18 h and cryoprotected in 30% glycerol overnight prior to freezing. The fixed animals were placed between two gold discs, plunged into liquid nitrogen-chilled isopentane, and placed into a double replica holder for a Balzer's 301 freeze etch device. The samples were cleaved within the freeze etch device by free breaks, shadowed with Pt/C to form a metal replica, and washed in bleach before mounting the replicas on slot grids for TEM.

Scanning Electron Microscopy (SEM)

L4 hermaphrodites were selected *en masse*, grown overnight (12–16 h) to the adult stage, and transferred to an unseeded plate to remove bacteria. The adults were transferred to a watch glass with 0.5 ml of 1× PBS. The worms were washed with one change of 1× PBS and gonads were dissected in 1× PBS containing 0.05% tricaine/0.005% tetramisole. The dissected gonads were transferred to a 6 × 50-mm borosilicate glass tube and the gonads were recovered by centrifugation at 1000 rpm in an IEC clinical centrifuge for 2 min at room temperature. The gonadal basal lamina was digested by incubation with 20–40 units/ml of Type II collagenase (Worthington Biochem Corp., Freehold, NJ) in 1× PBS for 2–12 min at room temperature. Following digestion, the gonads were placed on ice and the supernatant was gently removed from the gonads which had settled during the incubation period. The gonads are fragile until fixation and solutions were added slowly so that turbulent flows would not disrupt them. The gonads were washed with cold 1× PBS, allowing the gonads to settle by gravity. The gonads were then fixed with 3% glutaraldehyde in 0.1 M sodium phosphate buffer (pH 7.2) for 4 h on ice. Following fixation, the gonads were washed three times with cold 0.1 M sodium phosphate buffer (pH 7.0) containing 5% sucrose, incubating on ice for 15 min during each wash. Following the final wash, gonads were pipetted into a watch glass and intact gonads were hand selected with viewing under a dissecting microscope. The gonads were postfixed in 1% osmium tetroxide in 0.1 M sodium phosphate buffer (pH 7.2) for 1 h at room temperature. The gonads were then rinsed with several changes of 0.1 M sodium phosphate (pH 7.2) and dehydrated in an ethanol series (50, 70, 95, 100%). After a second change of absolute ethanol, the gonads were placed in the cooled chamber of a critical point drier with the samples covered with ethanol. To prevent the samples from being damaged when solvent entered or was vented from the chamber, we placed the gonads between several layers of filter paper cut with a standard hole punch. Dried samples were transferred to aluminum stubs covered with double stick tape using a camel hair brush and desiccated overnight and then coated with gold using a sputter coater. Gonads were examined in Hitachi S-4200 and S-500 scanning electron microscopes operated at 1–5 or 15–20 kV, respectively.

Since we were interested in correlating the length of the distal tip cell processes with the extent of the mitotic zone, it was important to determine the extent of the mitotic zone in the young adult stage (12–16 h post-L4) under our growth conditions (20°C). The original report defining the extent of the mitotic zone (Crittenden *et al.*, 1994) employed a growth temperature of 15°C. We quantitated the positions of mitotic nuclei relative to the distal tip cell in 49 young adult gonad arms, using anti-phosphohistone H3 antibodies to detect mitotic germ cell nuclei (prophase to early telophase) as described (Kadyk *et al.*, 1998). Our results were in agreement with those of Crittenden *et al.* (1995). On average, each gonad arm contained three mitotic nuclei which were found between 1 and 24 nuclear diameters from the distal tip cell (the average position was 10 nuclear diameters from the distal tip cell).

Fluorescence Microscopy

Young adult hermaphrodite gonads were dissected, fixed, and immunostained as described (Rose *et al.*, 1997) using rat polyclonal antibodies against the yolk proteins YP88, YP115, and YP170 (Sharrock, 1983, 1984), provided by Peg MacMorris (University of Colorado Health Science Center). MHCA expression in the gonadal sheath cells was detected using monoclonal antibody 5.6 as described (Rose *et al.*, 1997). Indirect immunofluorescence was visualized on a Zeiss Axioskop using a planApo 63× (NA 1.4) objective.

Sheath pair 1 were visualized using plim-7::GFP, a green fluorescent protein (GFP) reporter gene fusion to the *lim-7* homeobox gene (O. Hobert, unpublished data) located on cosmid C04F1 (also referred to as C04F1.3). plim-7::GFP was created by ligating a 4.13-kb *Pst*I–*Bam*HI genomic fragment into the pPD95.75 GFP reporter gene vector. This *lim-7::gfp* fusion gene contains 2.23 kb of 5′-upstream sequences, the first two exons, and the first intron of the *lim-7* gene, thus creating a fusion of the first 61 amino acids of LIM-7 to GFP, excluding the LIM domain and the homeodomain. Transgenic *C. elegans* lines were constructed by injecting plim-7::GFP at 50 μg/ml together with 100 μg/ml of the pRF4 dominant *rol-6(su1006)* marker gene (Kramer *et al.*, 1990) into wild-type animals as described (Mello and Fire, 1995). Five independent transgenic lines revealed similar patterns of expression in gonadal sheath cells 1–4 and in a few head neurons. Similar expression was observed using pJM24 (*lin-15*) as the coinjected marker. GFP fluorescence was visualized in living animals and also in dissected and fixed gonadal preparations using a Zeiss Axioskop with a planApo 100× (NA 1.4) objective and a Zeiss LSM410 confocal laser-scanning microscope. Dissected gonads from young adults (15 h post-L4) were isolated as described above, except that fixation was for only 20–30 min with 3% paraformaldehyde, in order to preserve GFP fluorescence. The distal extent of sheath cell 1 filopodia was analyzed in 39 young adult gonads in which the DNA was counterstained with 4′,6-diamidino-2-phenylindole (DAPI; Boehringer-Mannheim).

The length distribution of the dtc processes was evaluated using

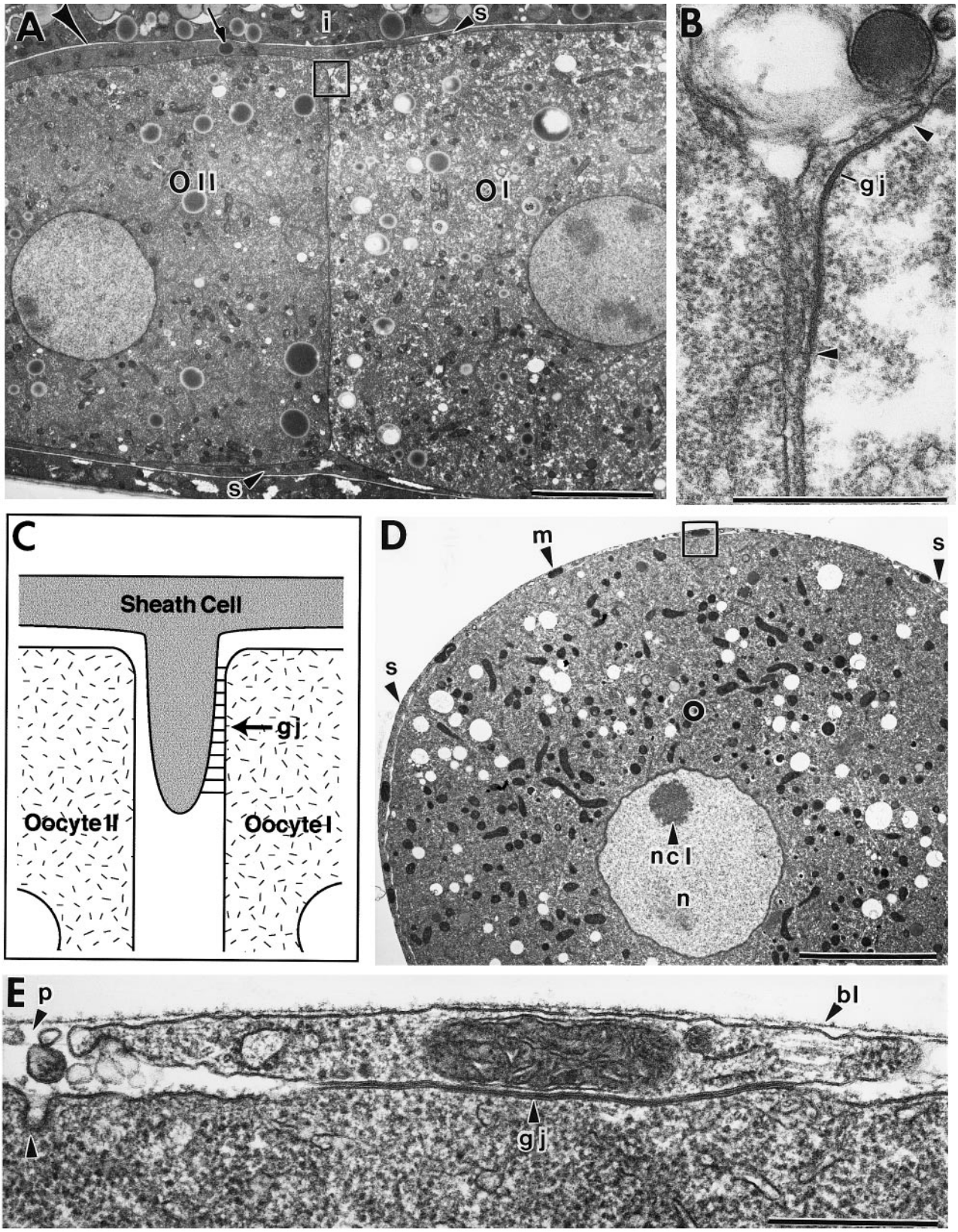

a *lag-2::gfp* fusion construct (Fitzgerald and Greenwald, 1995). Young adult gonads (15 h post-L4) were fixed and GFP fluorescence was analyzed as described above. All the dtc processes in a gonad arm that were visible by fluorescence microscopy were scored.

EM Immunocytochemistry (ImmunoEM)

Adult wild-type animals were lightly fixed in 4% paraformaldehyde or 2% glutaraldehyde in Hepes buffer under microwave irradiation for 10 min at approximately 4°C. Fixed animals were rinsed in buffer, embedded in 3% agarose in clusters, dehydrated through alcohols, and infiltrated with LR Gold resin at −20°C. Individual clusters were UV cured in gelatin capsules at −20°C overnight. Thin sections were collected on formvar-coated nickel mesh grids, and postembedding immunocytochemistry was performed using an anti-YP170 (yolk protein) antibody (Sharrock, 1983, 1984) provided by Barth Grant. A gold-linked secondary antibody (Amersham Auro-Probe, 10 nm gold) was used to visualize the anti-yolk antibody by electron microscopy. After antibody procedures, grids were rinsed, fixed with glutaraldehyde, and poststained with aqueous uranyl acetate (Hall, 1995).

Essentially the same results were obtained using a transgenic strain (DH1033) expressing a vitellogenin–GFP construct under control of a vitellogenin promoter (*vit-2::gfp*) to mark the location of yolk protein. The transgenic strain DH1033 *sqt-1(sc103); bIs1[vit-2::gfp + rol-6(su1006)]* was provided by Barth Grant (Columbia University). Three commercially available antibodies raised against GFP (RDI Research Diagnostics rabbit polyclonal, Quantum 11E5 mouse monoclonal, and Clontech rabbit polyclonal) were compared and all gave similar results. A full description of the EM immunocytochemistry procedures and a comparison of the different anti-GFP antibodies will be presented elsewhere (D. Hall, A. Miller, and M.-C. Paupard, in preparation).

RESULTS

Gap Junctions in the Proximal Gonad

Sheath/oocyte gap junctions. Using transmission electron microscopy, we observed gap junctions at sites of close apposition between proximal sheath cells and oocytes (Fig. 2). These junctions characteristically showed the following features: (1) plasma membranes become smooth and regular at regions of close apposition, with a narrow (~1 nm) extracellular gap between them; (2) at these junctions, each membrane is somewhat more electron dense than nonjunctional plasma membranes; and (3) the sheath/oocyte junctions are similar to gap junctions formed in other nematode tissues, but are among the largest found in any tissue (Hall, 1987; Buechner *et al.*, 1999; D. Hall, unpublished results). Sheath/oocyte gap junctions were observed at regions of extensive contact between sheath cell somata and oocytes (Figs. 2D and 2E). In addition, we observed gap junctions at sites where finger-like sheath cell processes extended between oocytes (Figs. 2A–2C). In the example shown, the junction is slightly twisted owing to the plane of section, but by tilting the specimen a uniform junctional apposition could be followed in serial thin sections between the two arrowheads in Fig. 2B.

Further verification of gap junctional identity and size was obtained by analyzing freeze-fracture replicas of sheath/oocyte membranes. After freeze fracture, gap junctions are identified as closely packed clusters of intramembrane particles and shallow pits (Fig. 3). During free cleaving of frozen tissue, the fracture plane tends to split the plasma membrane of a given cell into two complementary leaflets; the outer, exoplasmic leaflet is termed the E-face, while the inner, cytoplasmic leaflet is termed the P-face. A shallow pit is left behind in one membrane leaflet when a gap junction particle pulls away in the opposite leaflet. Thus, the pattern of particles and pits shows the placement of individual channels. Studies in vertebrates indicate that each particle corresponds to a multimeric connexon transmembrane channel, through which ions and small molecules flow (see review by Simon and Goodenough, 1998). According to the current model, the innexin gene family encodes gap junctional components in invertebrates (Phelen *et al.*, 1998a,b; see Discussion). There are about 20% particles versus 80% pits in these E-face views (Fig. 3). The ratio of particles to pits in the E-face or P-face membrane

FIG. 2. Gap junctions between oocytes and proximal sheath cells. (A) Low-magnification TEM of a longitudinal section of an intact adult hermaphrodite. The two most proximal oocytes (I and II) are shown in this panel with the most proximal oocyte (I) at the right. The cytoplasm of oocyte I has a lower electron density and an increased number and variety of organelles. The proximal sheath cells (small arrowheads) form a thin layer between the oocytes and the gonadal basal lamina. A thin pseudocoelom (clear space indicated with a large arrowhead) separates the gonadal basal lamina from the intestine (i) and body wall. A rare electron dense yolk granule within a sheath cell is indicated by an arrow. The box indicates the region from an adjacent section where a thin process from sheath cell 5 inserts between the oocytes and forms a gap junction with oocyte I (shown in more detail in B and schematized in C). (B) Sheath/oocyte gap junction (gj) formed between a finger-like sheath process and oocyte I. By tilting the stage in serial sections, the gap junction was found to extend the length of the region between the arrowheads (~0.6 μm). (C) Schematic representation of the sheath/oocyte gap junction shown in A and B. (D) Low-magnification TEM of a transverse section of a dissected gonad from a wild-type adult. The proximal gonadal sheath (s) forms a thin layer completely surrounding the oocyte except for the sheath pores (shown in more detail in Figs. 3 and 4). Several sheath cell mitochondria are evident (m). The oocyte nucleus (n) and nucleolus (ncl) are clearly visible This section was taken in the proximal arm and corresponds to oocyte II surrounded most likely by sheath cell pair 4. The box indicates the region where a sheath/oocyte gap junction is enlarged in E. A sheath/oocyte gap junction formed at a region of close apposition between the sheath cell and the oocyte. Note the delicate gonadal basal lamina (bl) and an open region corresponding to a sheath pore (p). The oocyte plasma membrane is observed to form a rare coated pit-like structure (arrowhead) adjacent to a pore. Scale bar corresponds to 5 μm in A and D and 0.5 μm in B and E.

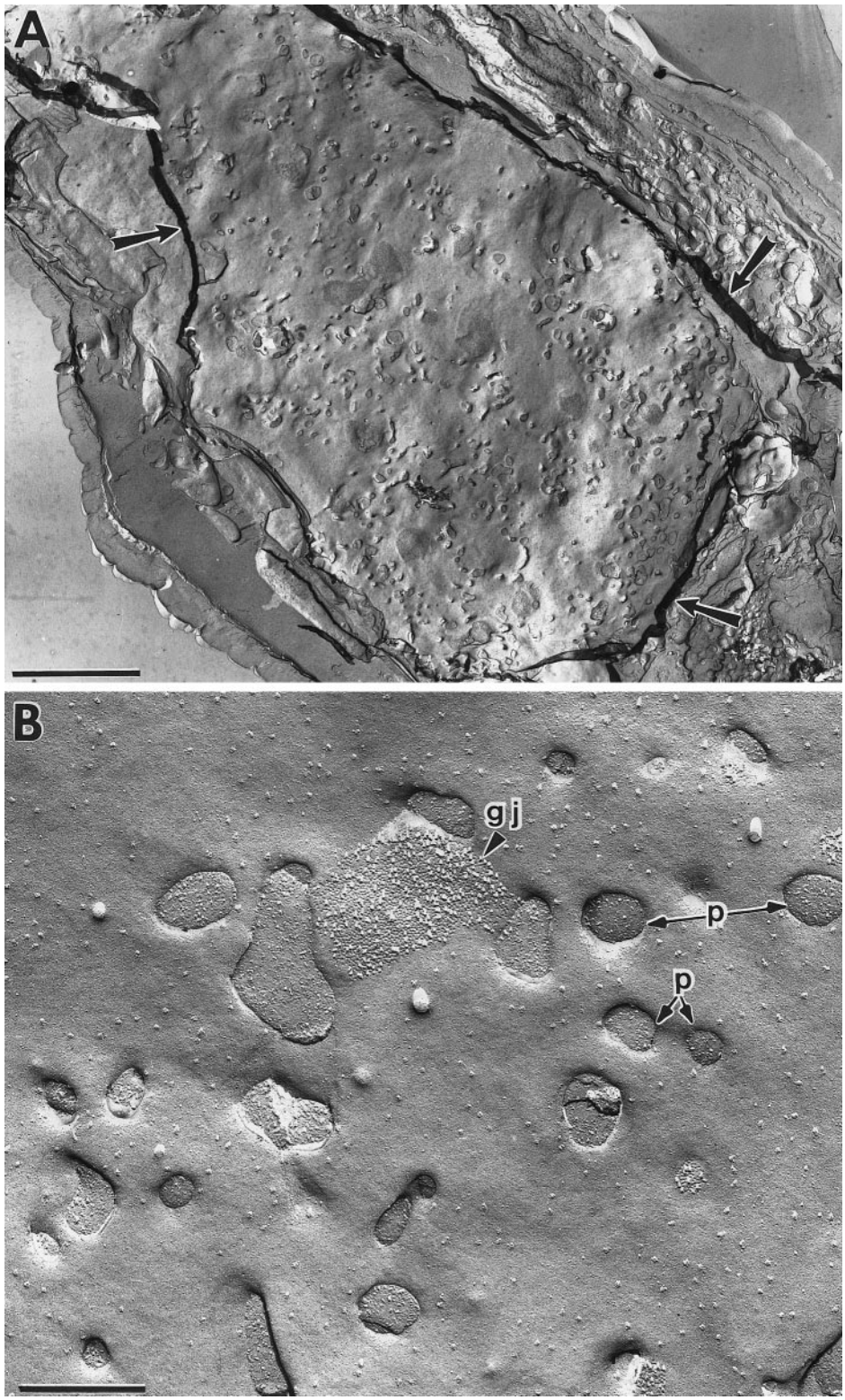

FIG. 3. Freeze-fracture replica of the proximal gonadal sheath. (A) Low-magnification image indicating the outlines of a proximal sheath cell 4 (arrows) covering oocyte II. The proximal boundary of sheath cell 4 is at the lower right. (B) High-magnification view of the sheath cell surface. Clustered intramembrane particles and pits on the E-face indicate a gap junction (gj). Irregular sheath pores (p) form fenestrae through which the oocyte surface is visible. Scale bar corresponds to 5 μm in A and 0.5 μm in B.

leaflets is known to vary from tissue to tissue in *C. elegans* and in other invertebrate gap junctions, whereas in vertebrate gap junctions all particles cleave to the P-face (Hall, 1987; Quick and Johnson, 1977). Diameters of sheath/oocyte gap junction profiles in these preparations were comparable to values obtained by thin-section analysis (300–1000 nm). The relatively large size of these structures could reflect the similarly large size of sheath cells and oocytes, or they could permit high-capacity intercellular exchange of small molecules and ions.

Sheath/sheath gap junctions. Where adjoining sheath cell processes overlap, prominent gap junctions often form between them (Fig. 4A). Gap junctions were observed between members of individual sheath cell pairs (e.g., 4–4) as well as between adjacent sheath cells (e.g., 4–5). As with sheath/oocyte gap junctions, the profile lengths of sheath/sheath gap junctions are large (~0.3–1.7 μm). No tight junctions or septate junctions between sheath cells were observed, nor were any associations with neurons. Occasional adherens junctions were also noted in the proximal sheath between apposing sheath cells (data not shown). An attractive possibility is that due to their large size, sheath/sheath gap junctions (and occasional adherens junctions) may also play a structural role to anchor adjoining sheath cells in regions of contact. Previous work established that the POU-homeobox gene *ceh-18* is required for the normal differentiation and function of the proximal sheath cells (Greenstein *et al.*, 1994; Rose *et al.*, 1997). In contrast to sheath/oocyte gap junctions which were rare or absent in *ceh-18(mg57)* animals, sheath/sheath gap junctions were observed and appeared similar to the wild type (data not shown). Thus, a dearth of sheath/oocyte gap junctions may contribute to defects in meiotic maturation and ovulation observed in *ceh-18* mutants.

Muscle-like Features of the Proximal Sheath Cells

Sheath cell contractions drive ovulation (Ward and Carrel, 1979). Sheath cells contain thin and thick filaments (Hirsh *et al.*, 1976; Strome, 1986) and express myosin heavy chains A and B (Strome, 1986; Rose *et al.*, 1997). Consistent with these observations, analysis of mutants suggests that sheath cell contractions are an actomyosin-dependent process (Myers *et al.*, 1996; McCarter *et al.*, 1997; Rose *et al.*, 1997). Sheath cell myofilament bundles are arranged longitudinally and circumferentially. Individual filament bundles are long and very narrow with few filaments per bundle, when compared to body wall muscle sarcomeres (see Moerman and Fire, 1997, for a review of body wall muscle structure).

Electron-dense plaques on the cytoplasmic face of the sheath cell plasma membrane are associated with the bundles (Figs. 4B and 4D), always on the cell's basal surface. We refer to these electron-dense plaques as hemi-adherens junctions. The rationale for this classification is presented below and in the Discussion. The closest myofilaments to each hemi-adherens junction are always thin, not thick filaments. In favorable views, the thin filaments appear to project obliquely to the plasma membrane at hemi-adherens junctions; thus, they are likely to serve as attachment points for thin filaments. The gonadal basal lamina appears to attach more closely to the plasma membrane at these junctions (Figs. 4B and 4D). Hemi-adherens junctions are more readily observed by TEM in dissected gonad preparations because of their enhanced contrast compared to intact animals. Hemi-adherens junctions are common in sheath cell pairs 3–5, but not in pairs 1 and 2. Since these sheath junctions appear to associate with microfilaments, they are more properly related to adherens junctions than desmosomes (Lane and Flores, 1990; Tepass and Hartenstein, 1994). Similar junctions are present in pharnygeal muscles, where they were previously termed "half desmosomes" (Albertson and Thomson, 1976), and much more elaborate membrane junctions, called dense bodies, are well described in body wall muscles (Francis and Waterston, 1985; see Discussion). We propose that hemi-adherens junctions function to anchor the myofilament apparatus within the basal plasma membrane of the sheath cell and to the exterior basal lamina.

Sheath Pores Permit Yolk Transfer to Oocytes

Detection of sheath pores by TEM. Small discontinuities or gaps (0.1–0.2 μm) in the sheath cell coverage of oocytes are very common in the proximal arm (Fig. 4C). In TEM images of dissected gonadal preparations, these small gap regions have the appearance of conduits between the gonadal basal lamina and oocytes. Serial-section TEM analysis of intact gonads suggests that the gap regions are actually small holes in individual sheath cells, which we have termed sheath pores. The nature of sheath pores was further explored by two independent EM techniques, which better demonstrate their frequency and size range.

Detection of sheath pores in freeze-fracture replicas. Sheath pores are also apparent in freeze-fracture images of the gonad sheath with the underlying oocyte membrane visible through the pore (Fig. 3). The size distribution (0.1–0.3 μm) and scatter (1–2 pores/μm^2) of sheath pores appear to be equivalent by freeze fracture and SEM. There is some indication that pores may be grouped into clusters, separated by regions dominated by intercellular junctions.

Detection of sheath pores by SEM. To visualize the surface of sheath cells by SEM, we modified methods for observing the surface of myoepithelial cells from vertebrate exocrine glands (Nagato *et al.*, 1980). SEM images demonstrate that the proximal sheath cells form a thin covering over oocytes. The sheath is so thin that its outside topography closely follows the undulations of underlying single oocytes (Fig. 5E). Multiple small indentations on the surface of proximal sheath cells from dissected gonads (Figs. 5E–5I) correspond to the sheath pores visualized by TEM. In some preparations, the samples were damaged in handling such that the thin sheath detached or ripped (Figs. 5G–5I), resulting in a stretching of the sheath pores much as occurs when gauze is stretched. Nevertheless, this was informa-

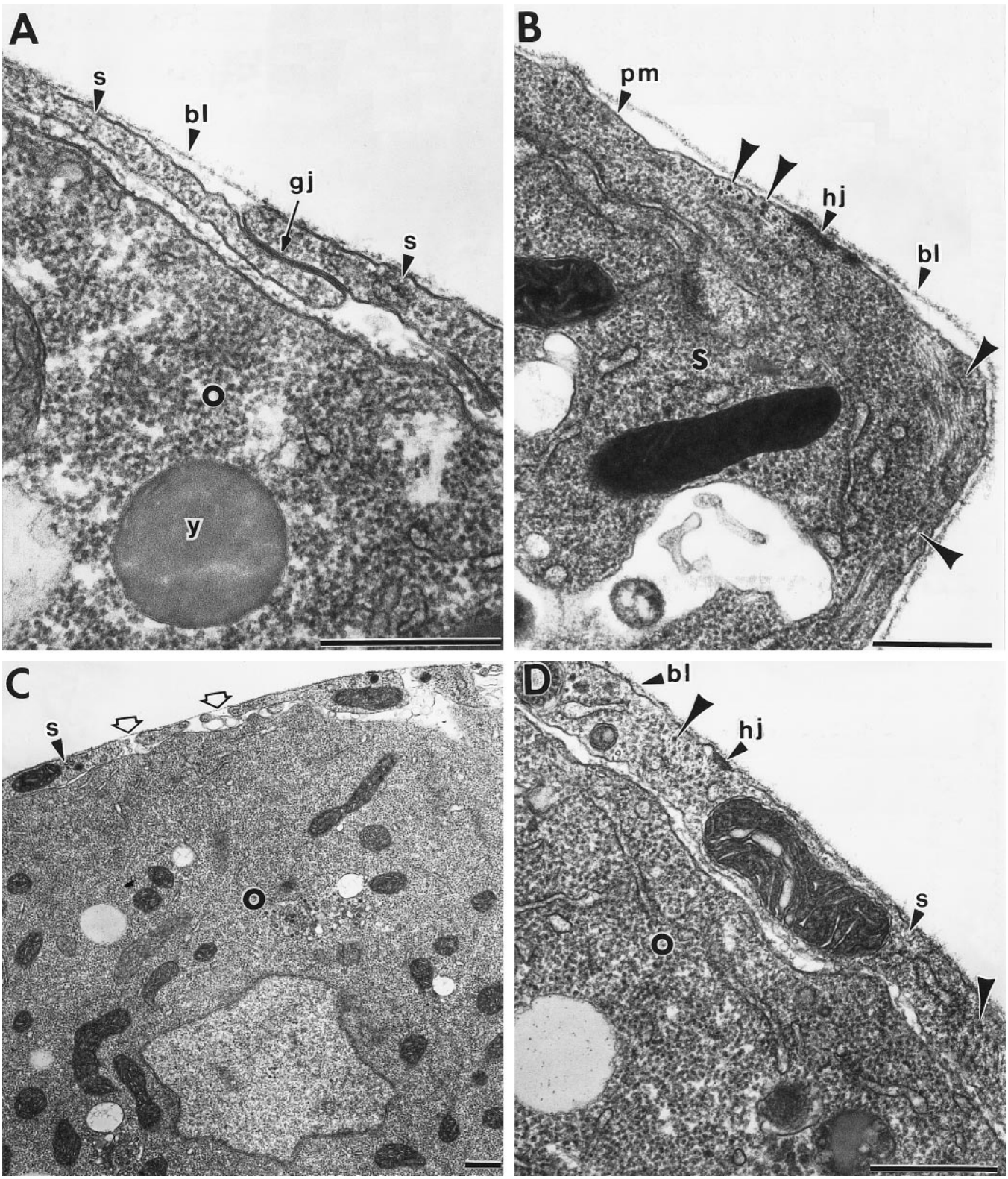

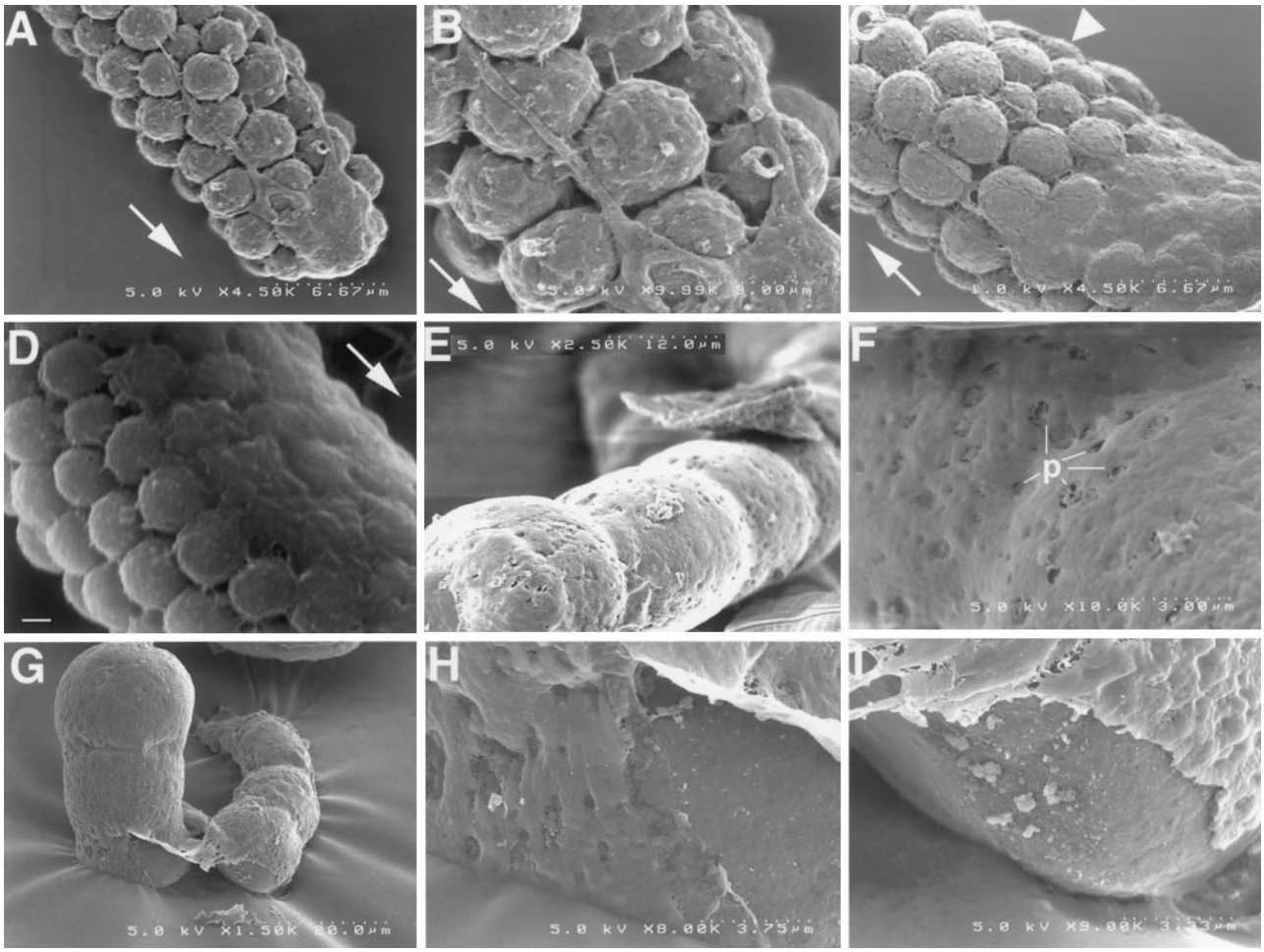

FIG. 5. Scanning EM views of dissected gonadal preparations from wild-type adult hermaphrodites (12–16 h post-L4). The gonadal basal lamina was digested using collagenase treatment, permitting the visualization of the surface of somatic gonadal cells and germ cells (round objects). (A, B) The distal tip cell (dtc) surface. The soma of the dtc lies at the extreme distal tip of the gonad arm tightly wrapping over the germ cells, with thin processes extending at least 10 germ cell diameters along the proximal–distal axis. An arrow points in the distal direction in A–D. (C, D) Visualization of the distal gonad arm and sheath cell 1. Sheath cell 1 extends thin filopodia that end approximately 15 to 30 cell diameters away from the distal tip. This results in an unsheathed or "bare" distal region indicated by an arrowhead in C. It is important to emphasize that the germ cells in this bare region are normally covered by the gonadal basal lamina which was digested for SEM analysis. Each filopodium tends to run distally, in a groove between germ cells, with some evidence for thinner lateral strands pressing into the groove. Note that each individual sheath cell 1 only covers one face of the gonad and the surface of bare germ cells is seen adjacent to the margin of sheath cell 1 (D). By rotating the sample, the margin of the sheath cell could be visualized. (E, F) The surface of the proximal gonad arm. Sheath cells (3–5) are seen in low-power (E) and high-power views (F). Sheath pores (p) are seen as indentations in the surface of the sheath. By this method, the proximal sheath cells appear to completely cover the proximal gonad arm, consistent with TEM results. (G–I) Some samples exhibited evidence of mechanical damage, which were nevertheless illuminating concerning the structure of the proximal arm. In low-power (G) and high-power views (H, I), the sheath appears to have been torn and lifted, revealing the surface of the large oblong oocytes beneath. In I, the sheath pores appear to have been stretched. Micrographs in A–C and E–I were taken in an Hitachi S-4200 scanning electron microscope. The beam voltage and the magnification are indicated. The micrograph in D was taken on an Hitachi S-500 scanning electron microscope and its scale bar corresponds to 1.5 μm.

FIG. 4. Ultrastructure of proximal gonadal sheath cells. TEM images of sheath cells (s) and oocytes (o) from transverse sections of dissected gonadal preparations from wild-type hermaphrodites (A–D). (A) Sheath/sheath gap junction (gj) formed at a region of contact of two adjacent proximal sheath cells. A membrane-bounded electron-dense yolk granule (y) is observed within the oocyte cytoplasm. The gonadal basal lamina (bl) is indicated. (B, D) A sheath cell with a hemi-adherens junction (hj) formed adjacent to the gonadal basal lamina (bl). Cross-sectional and tangential profiles of thick and thin filaments (arrowheads) are seen adjacent to the sheath plasma membrane (pm) and the hemi-adherens junction. Thin filaments cluster very close to the hemi-adherens junction, while others are interspersed between thick filaments. (C) Sheath pores are seen in cross-section as breaks in the sheath cell coverage (open arrows) of oocytes. The pores extend from the gonadal basal lamina to the oocyte surface. Scale bar corresponds to 0.5 μm in A, B, and D and 1.0 μm in C.

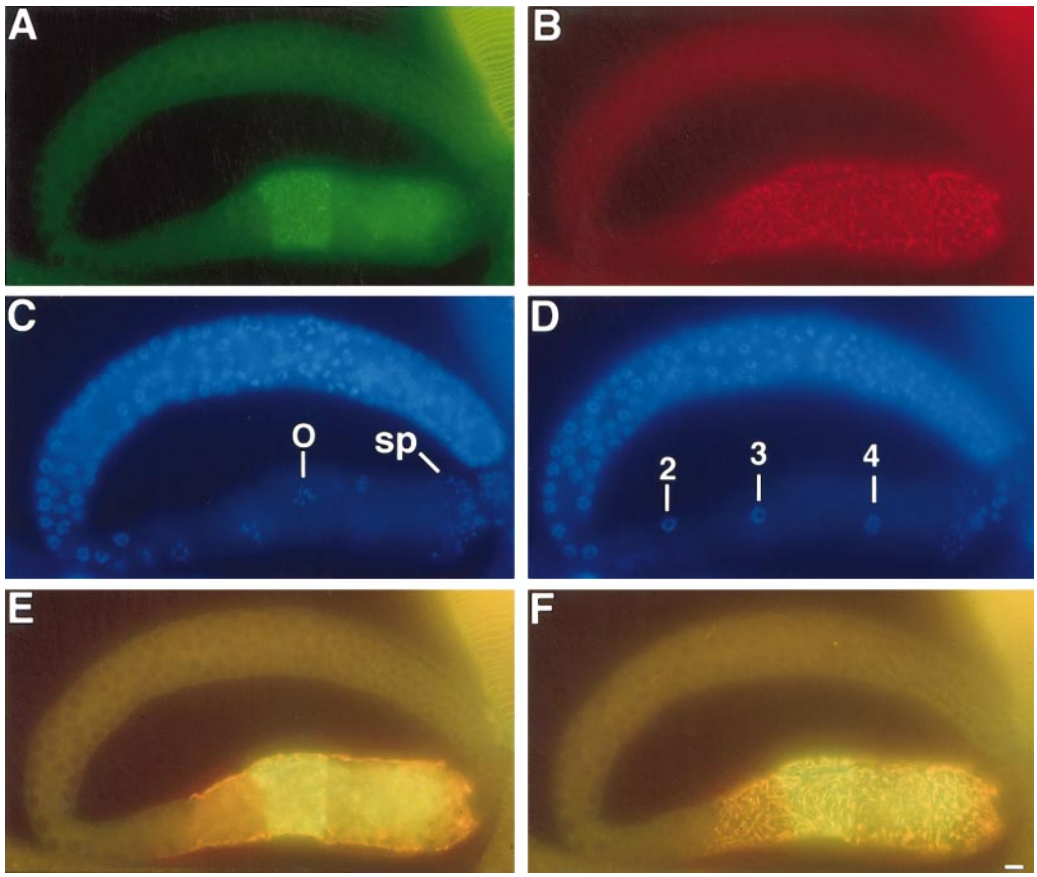

FIG. 6. Yolk proteins are found within oocytes, not sheath cells. Gonads dissected from wild-type adult hermaphrodites were stained with polyclonal antibodies against a constituent of yolk particles (yp170) and monoclonal antibodies against myosin heavy chain A (MHCA). yp170 expression was detected by FITC staining (green) (A, E, F) and MHCA expression was detected by rhodamine staining (red) (B, E, F). Double exposures were prepared in E and F to ascertain whether the yp170 staining and the MHCA staining colocalized. DNA was detected using DAPI staining (C, D). The same specimen is shown in different focal planes in each panel as follows. (A, C, E) A medial optical plane displays the oocyte bivalents in clear focus (O). Sperm in the proximal arm are also indicated (sp). (B. D. E) A superficial optical plane displays the proximal sheath cells. Photographs in B and F were taken such that the sheath myofilaments were in clear focus. D was taken in a slightly lower plane of focus to visualize the sheath nuclei (labeled 2–4) which lie nestled just beneath the myofilaments. Note that sheath cell 2 contains few myofilaments. By observing the sample in multiple planes, the yolk protein immmunoreactivity appeared to localize within the oocyte and at the oocyte surface, but not within the sheath cell. Scale bar in F corresponds to 10 μm. Similar results were also obtained with antibodies to YP88 and YP115 (data not shown). The specificity of staining was assayed by staining gonads dissected from adult males which do not synthesize yolk (Doniach and Hodgkin, 1984; Shen and Hodgkin, 1988) and do not stain with these antibodies. In some experiments faint staining was observed in the distal arm.

tive, directly demonstrating the thinness of the sheath and its close apposition to the oocyte.

Yolk transport through sheath pores. Yolk proteins are synthesized by the intestine and transported into oocytes (Kimble and Sharrock 1983) by an unknown mechanism. The gonad is separated from the intestine by an intervening fluid-filled pseudocoelom, which contains isolated free yolk particles in wild-type adults. To be transported into oocytes, yolk particles from the intestine must first traverse the gonadal basal lamina and proximal sheath cells. We considered the possibility that yolk particles are actively taken up by sheath cells and are then transported to oocytes. However, this appears not to be the case because electron-dense yolk granules are very rarely observed within sheath cells by TEM (see Fig. 2A). To further test whether yolk can be found in sheath cells, we examined the distribution of yolk protein immunoreactivity in sheath cells and oocytes by indirect immunofluorescence in dissected gonadal preparations (Fig. 6). At the limits of resolution of this method, yolk protein immunoreactivity is found within oocytes but not sheath cells, with the most intense staining limited to optical planes beneath the sheath cell myofilaments. This conclusion is supported by TEM analysis on intact gonads (see below). It should be noted that TEM analysis suggests that the total yolk particle content in dissected preparations is likely to be re-

duced compared to the intact gonad, probably due to exposure of the dissected gonad to the medium prior to fixation. This minimizes the chance that extracellular yolk particles could be viewed within sheath pores by immunofluorescence and increases the contrast between the yolk-poor sheath and the yolk-rich oocyte cytoplasm. Furthermore, TEM analysis of yolk particle distribution in several mutants in which oocyte development is defective due to gonad disorganization (e.g., *epi-1* and *epi-2*) indicates that yolk accumulates in the pseudocoloem but not in sheath cells or the germ line (D. Hall and E. Hedgecock, unpublished results). Thus, when yolk transport to oocytes is blocked or reduced, as an indirect consequence of defects in oogenesis, yolk granules do not accumulate in the proximal sheath cells, although they do accumulate in the hypodermis. TEM of the *vit-2::gfp* strain, which overproduces yolk protein, reveals some yolk granule accumulation in other tissues, including hypodermis and muscle, but little in sheath cells (D. Hall, B. Grant, and M.-C. Paaupard, unpublished results). Taken together, these results suggest that transcytosis is not the major route of yolk uptake into the gonad.

In thin-section analysis of intact worms, electron-dense yolk particles were commonly associated with the sheath pores (Fig. 7). This material is not found within the sheath cell somata, but rather fills the space between the gonadal basal lamina and the oocyte plasma membrane and between sheath cells and oocytes. In some regions, the electron-dense material is associated with out-pocketings (and some in-pocketings) of the oocyte membrane (Fig. 7A). We speculate that these out-pocketings reflect recruitment of endocytotic machinery. A thin layer of flocculent material often coats the cytoplasmic surface of these out-pocketings, suggestive of a clathrin-mediated uptake mechanism (Mukherjee *et al.*, 1997). An omega-figure with a dense coating on the cytoplasmic surface was also observed on the plasma membrane of a full-grown oocyte from a dissected gonad in a region adjacent to a sheath pore (Fig. 2E), suggestive of endocytosis.

Within oocytes, electron-dense yolk material is membrane-bounded. We refer to the extracellular non-membrane-bounded electron-dense material as yolk particles and the intracellular, membrane-bounded material as yolk granules. These membrane-bounded osmiophilic granules have a similar appearance to presumptive yolk granules in intestinal cells (see Fig. 2A). The limiting membrane around a yolk granule is best viewed at high magnification and is not evident in glancing sections where the membrane is cut obliquely. It is interesting to note that in TEM of dissected gonadal preparations the electron-dense presumptive yolk particles within sheath pores are absent and only what appear to be remnants persist. Possibly this material is readily lost prior to fixation following the dissection procedure, as might be expected for extracellular material that fills the pores.

To further characterize the appearance of yolk protein aggregates within cellular organelles and in the pseudocoelom, immunoEM was used. Virtually the same results were obtained by two methods: (1) using an anti-yolk protein antibody on wild-type hermaphrodites and (2) using an anti-GFP antibody on the *vit-2::gfp* strain (DH1033) in which the intestine synthesizes both vitellogenin and a vitellogenin–GFP (VIT-2–GFP) fusion protein. The primary antibodies were identified in the TEM using gold-labeled secondary antibody. Consistent with the TEM results presented above, yolk protein immunoreactivity lies primarily within electron-dense membrane-bounded organelles in full-grown oocytes (Fig. 8) and in the intestine (data not shown). These labeled yolk granules are more electron dense than other organelles in either tissue, thus confirming our ability to identify yolk protein aggregates in normal tissue. Large electron-dense particles in the pseudocoelom were also labeled, confirming that these particles contain yolk protein (Fig. 8). Young animals, such as L2 larvae, which are at a developmental stage where endogenous yolk production has not yet begun (Kimble and Sharrock, 1983), showed no immunogold labeling in the intestine or elsewhere. In wild-type gonads, the anti-yolk antibody labeled many particles in close association with the proximal sheath cells, in nearby portions of the pseudocoelom, in sheath pores, and between the sheath and underlying oocytes (Fig. 8). In the *vit-2::gfp* strain, there was relatively little free yolk near the gonad sheath or in the pseudocoelom, as the majority of the immunoreactivity seemed to collect in enlarged particles within the intestine (data not shown). By immunoEM, we could not exclude the possibility that some yolk lay inside the sheath cell proper, as its cell membranes were not well preserved by the very light fixation protocol needed to preserve yolk protein antigenicity. However, the study of well-fixed tissue by TEM (see above) indicates that internalization of yolk protein by proximal sheath cells is very rare.

Distal Sheath Cells Extend Filopodia over the Bare Gonad Arm

We analyzed the ultrastructure of the distal sheath cells using SEM (Fig. 5) and TEM (Fig. 9). In addition, a GFP promoter fusion permitted the direct visualization of sheath cell pair 1 in living animals and in dissected gonadal preparations using conventional fluorescence microscopy and laser-scanning confocal microscopy (Fig. 10). Together, these methods have resulted in a consistent description of the distal sheath cells.

In contrast to proximal sheath cells, pair 1 (located in the distal arm) and pair 2 (located at the loop) contain very few thick filaments (Fig. 9) and are not visibly contractile by light microscopy of intact living animals. Sheath pairs 1 and 2 contain prominent endoplasmic reticulum and Golgi apparatus (Fig. 9A) leading us to speculate that these cells may have a secretory function. Sheath pair 2 completely ensheathes the loop region. By contrast, sheath pair 1 does not completely ensheath germ cells (Figs. 5C, 5D, 9, and 10). In the distal arm there are bare regions where the germ cells are unsheathed, covered only by a basal lamina. There

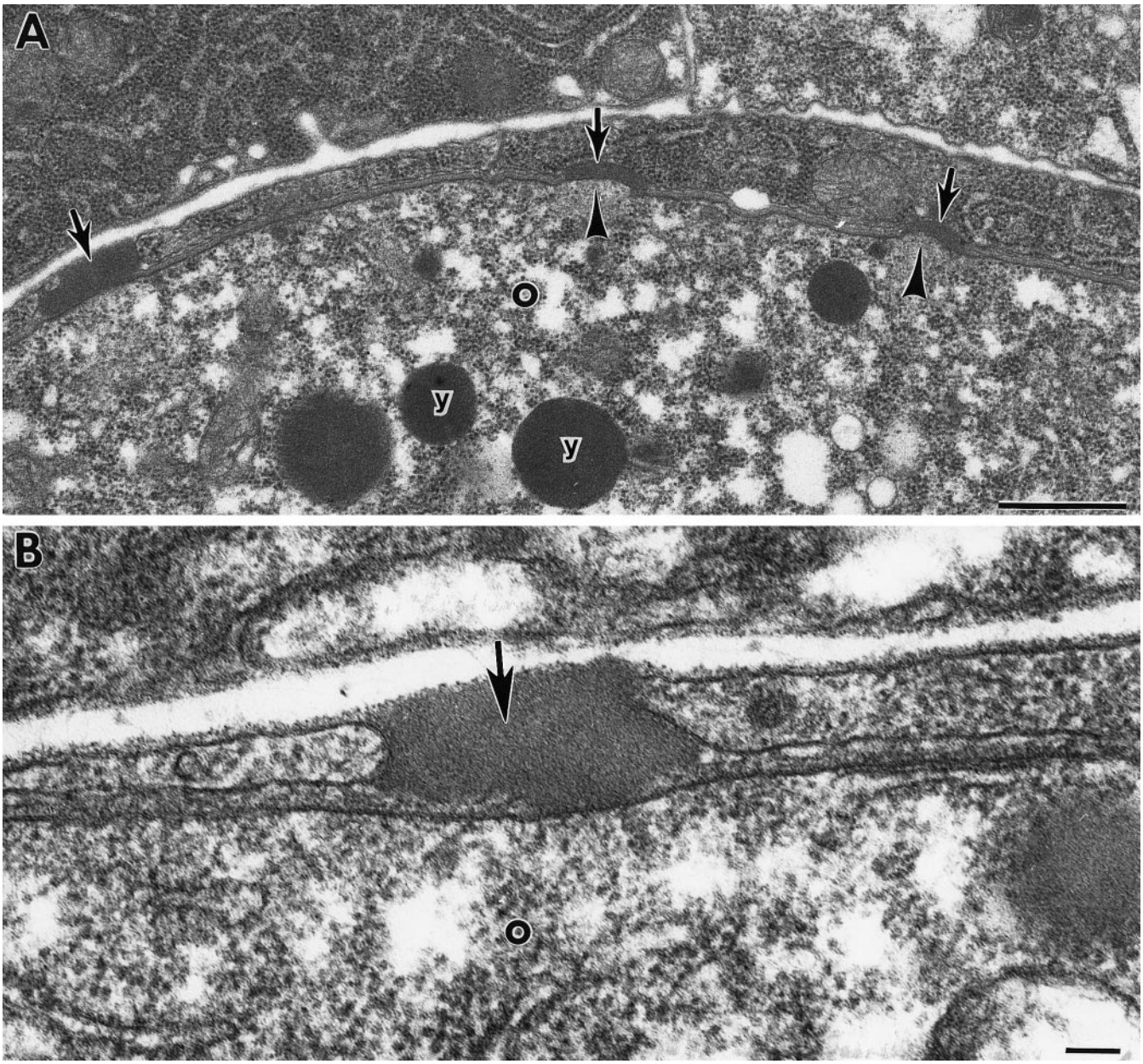

FIG. 7. Yolk transport through sheath pores and endocytosis. Low- (A) and high- (B) magnification TEM from wild-type adults. A is a transverse section, while B is longitudinal. Electron-dense yolk particles (indicated by arrows) are seen against the surface of the oocyte (o). Yolk particles in contact with the oocyte are associated with out-pocketings of the oocyte plasma membrane (arrowheads), where the underlying cytoskeleton looks diffuse and flocculent. In B, a yolk particle (arrow) fills a sheath pore and extends from the gonadal basal lamina to the surface of the oocyte. Note that yolk granules (y) within the oocyte appear to be membrane-bounded, except when viewed in glancing sections (dark circles in the oocyte in A), in contrast to the extracellular particles which lack membranes. Scale bars correspond to 1 μm in A and 0.1 μm in B. On rare occasion we have observed electron-dense yolk particles beneath the sheath of the distal arm, but this material was not taken up into distal germ cells (data not shown).

are bare regions both at the distal margins of each sheath cell 1 (Figs. 5C and 10) and between the two pair 1 sheath cells which cover opposite faces of the distal arm (Fig. 5D). In addition, there are patchy bare spots where each sheath cell 1 forms a ragged border. In SEM, the distal edge of sheath cell 1 displays finger-like filopodia extending into the bare region (Fig. 5C), often intercalated between the germ cells, at their outer edge. We have observed that the

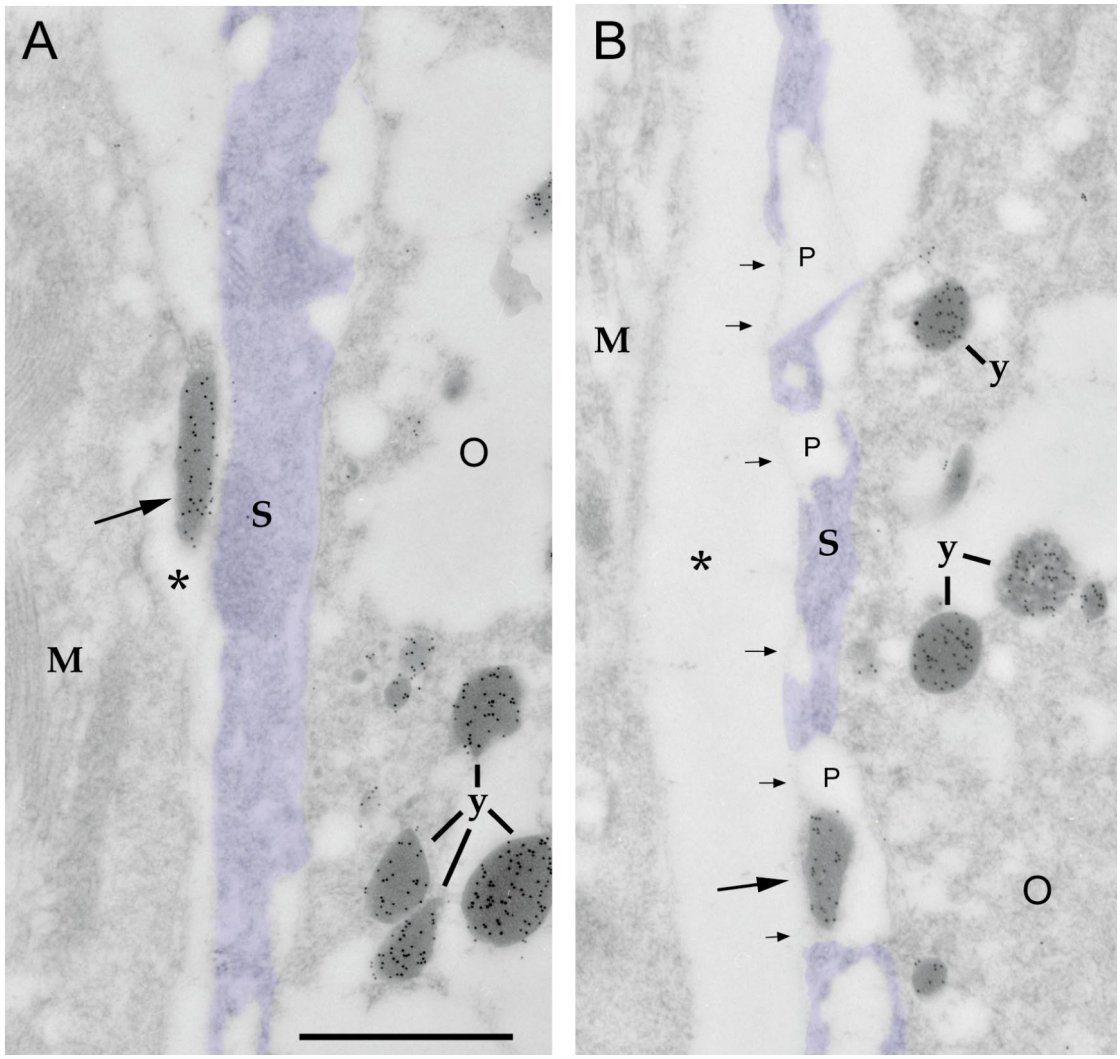

FIG. 8. ImmunoEM localization of yolk protein. (A) Thin section of an adult wild-type hermaphrodite shows specific immunogold label over electron-dense granules in an oocyte (O) and over an electron-dense particle (arrow) in the pseudocoelom (asterisk). Electron-dense yolk granules (y) within the oocyte contain immunogold label. (B) A nearby portion of the same animal showing a labeled yolk particle (large arrow) which lies in an open sheath pore (p). A thin basal lamina covers the outer edge of each pore (indicated by small arrows). Since plasma membranes were indistinct owing to the light fixation necessary to preserve antigenicity, the sheath has been false-colored to accentuate its relationship to the oocyte. Note that the immunogold label is very rarely found within sheath cells (S) or body wall muscles (M). Scale bar corresponds to 1 μm.

distal sheath filopodia can project four germ cell diameters from the sheath border (see Fig. 5C). Similarly, TEM of transverse sections show that in addition to a flattened soma pressed into the gonad, the volume of each sheath cell 1 cytoplasm is concentrated into wedges that insert between germ cells (Figs. 9B and 9C). By contrast, an extremely thin sheath covers the top of most germ cells. Consistent with these TEM results, GFP expression in sheath pair 1 results in a honeycomb pattern (Fig. 10). The clear regions in the honeycomb pattern correspond to regions where an extremely thin sheath covers the germ cells and thus the GFP reporter is below the threshold of detection. Distal sheath filapodia were observed as thin wisps of GFP fluorescence at the distal margins of sheath cell 1 (Fig. 10). The distal-most extent of sheath cell 1 filopodia was analyzed by fluorescence microscopy in 39 gonads and found to reach approximately 19 $\pm$ 6 germ cell diameters from the distal tip of the gonad. A movie of projections of confocal sections of the distal sheath cells can be viewed at http://www.academicpress.com/www/journal/db/dbsupp.htm.

TEM analysis of serial sections shows that the filapodia extend directly from the wedges of sheath cell cytoplasm that insert between germ cells. Small clusters of thin filaments are commonly seen running lengthwise, at the

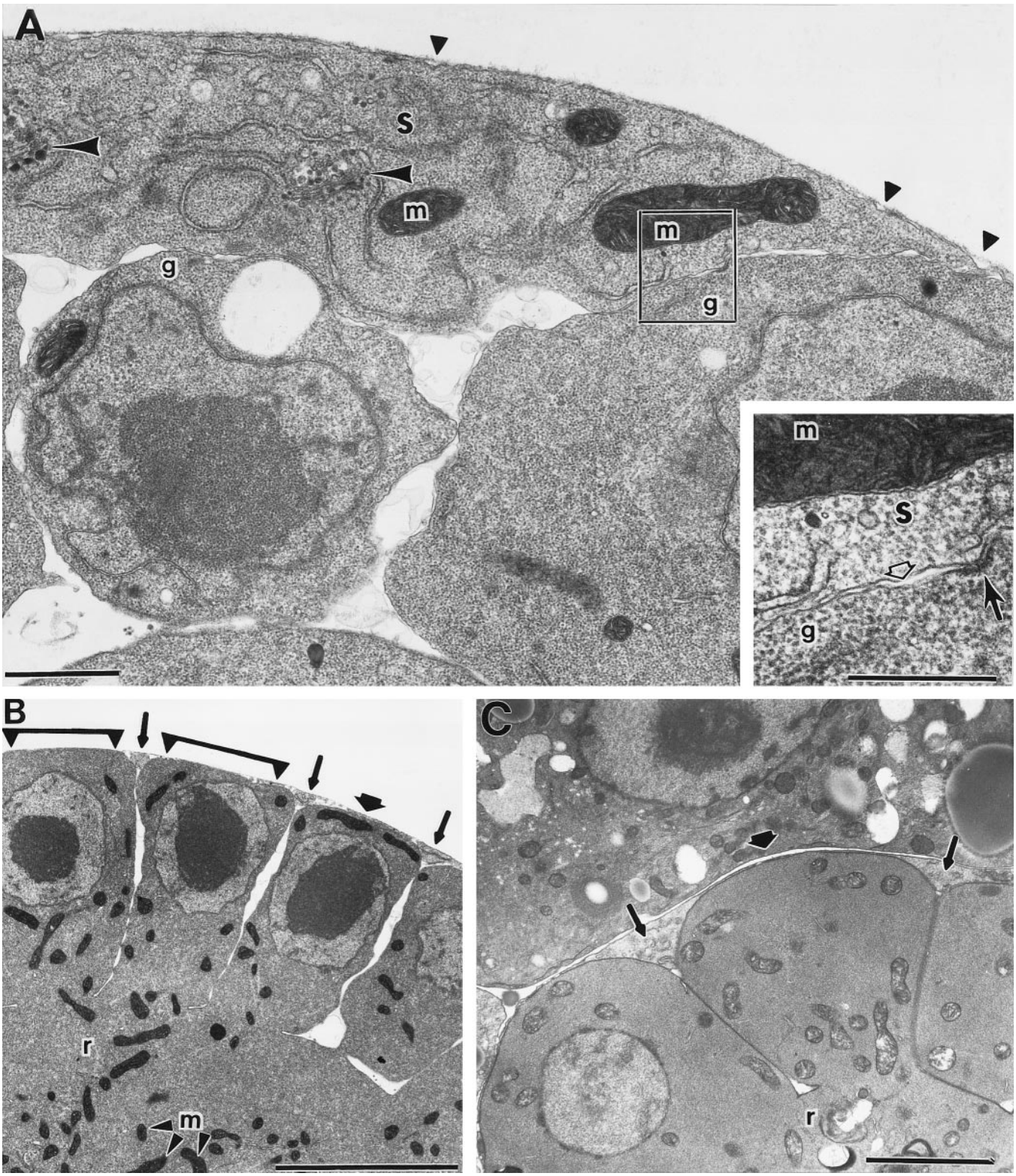

FIG. 9. Electron microscopy of distal gonad sheath cells. (A) Oblique/longitudinal section of a dissected gonad from a wild-type adult at the loop region. Distal sheath cell 2 (s) contains prominent Golgi apparatus (arrowheads), endoplasmic reticulum, some densely staining vesicles, and mitochondria (m). There are several clusters of small dark staining vesicles, mostly located at the fringes of the Golgi stacks. The gonadal basal lamina (indicated by solid triangles) lies outside the sheath and not between the sheath and the germ line (g). The boxed

deepest edge of insertion of sheath cell 1 between the germ cells (data not shown). These cytoskeletal elements likely strengthen the sheath cell as it envelops the outer surface of the germ cells in a space-filling manner, converting the bumpy texture of the germ line into a smooth outer surface (see Figs. 5C, 5D, and 9). Tangential images of the sheath's apposition to the germ line also show a high density of filaments projecting toward the plasma membrane (data not shown). These cytoskeletal elements might attach to the plasma membrane in order to anchor the sheath to the germ line over a broad footing.

Sheath filopodia generally are closely apposed to the outer surface of the germ line, with the basal lamina remaining closely adherent. Rarely, some filopodial branches extend more deeply between adjoining germ cells, approaching the rachis. In thin sections, they appear to be gradually tapered to a narrow tip (data not shown).

In contrast to proximal sheath cells, the distal sheath cells (sheath cell pairs 1 and 2) do not have organized systems of pores (Figs. 5C, 5D, and 9, and data not shown), although there are often larger ragged breaks in the covering of individual germ cells. We have not observed gap junctions between germ cells and distal sheath cells. However, we have observed sheath/sheath gap junctions in the distal arm (data not shown). In addition, there are structures resembling focal adhesions at regions of close apposition between sheath cells and germ cells (Fig. 9A). These rare junctions have an asymmetric appearance in that the germ cell junctional face appears more electron dense (Fig. 9A).

Distal Tip Cell Processes

The distal tip cell (dtc) regulates germ cell mitosis and entry into meiotic prophase (Kimble and White, 1981; Austin and Kimble, 1987; Kadyk and Kimble, 1998). In the wild type, mitotic nuclei are limited to approximately the first 24 germ cell diameters from the dtc, the mitotic zone (Crittenden *et al.*, 1994). Previously, Fitzgerald and Greenwald (1995) reported that the dtc extends processes based on immunofluorescence visualization of a *lag-2::gfp* fusion expressed in the dtc. Consistent with these observations, we have directly visualized the dtc soma and its thin processes using SEM (Figs. 5A and 5B). The dtc sits octopus-like over the tip of the gonad, firmly gripping the leading few germ cells, with tentacle-like processes trailing loosely behind. The dtc crawls along the body wall "headfirst." By SEM, the dtc processes appear to extend at least 10 cell diameters along the distal–proximal axis. The trailing edge of the dtc soma indents into the germ cells (Fig. 5B) suggesting a close association under pressure. The dtc processes appear to follow the contours of the germ cells (see Figs. 5A and 5B). At the distal extreme of the gonad shown in Figs. 5A and 5B, every germ cell is located within ~2 cell diameters from a dtc process. We have not observed the dtc processes to overlap the distal filopodia of sheath cell 1 by SEM or TEM, but cannot exclude the possibility that this can occur. In serial section analysis by TEM, the dtc processes in L4 larvae extend for approximately 3–5 cell diameters, with fragmentary material trailing further behind proximally as discontinuous blobs which appear to be shed by the dtc processes (data not shown, D. Hall and E. Hedgecock, unpublished results). To better evaluate the length distribution of the dtc processes, we analyzed *lag-2::gfp* (Fitzgerald and Greenwald, 1995) expression in dissected gonads ($n = 69$) from young adults and found that dtc processes ($n = 136$) extend on average 8 ± 4 germ cell diameters from the distal tip (range 2 to 20). Therefore, the SEM, TEM, and fluorescence data suggest that the dtc processes tend to be shorter than the maximal extent of the mitotic zone.

DISCUSSION

Electron microscopic analysis of the adult hermaphrodite gonad has revealed several ultrastructural features (e.g., gap junctions, sheath pores, sheath hemi-adherens junctions, adherens junctions, and distal sheath filopodia) not previously reported for this tissue (see Fig. 11 for a summary). Ultimately, mutational analyses will be critical for establishing the roles of these structures in the reproductive functions of the gonad. Below, we discuss briefly the potential functional roles of these structures in the context of wild-type development as a guide for future studies.

region in A is magnified in the inset to show a junctional structure that resembles a focal adhesion (indicated by a solid arrow) between the distal sheath cell and a developing oocyte. Note that in the inset there is no basal lamina found between the germ line (g) and the sheath (s) when viewing at high magnification. However, there is a small extracellular space (indicated by an open arrow) adjacent to the junction. Cross-sections of the distal arm from dissected (B) and intact (C) animals. The germ cells are covered by a thin basal lamina and connect to the anucleate core or rachis (r) to form a syncytium. The cytoplasm of sheath cell 1 is seen as wedges between germ cells (arrows). Mitochondria (m) are present within the rachis and in the syncytial germ cells. Germ cells that are apparently unsheathed are indicated by a bracket, whereas thinly sheathed germ cells are indicated by a short arrow. The two germ cells on the left are apparently unsheathed as the sheath cell cytoplasm does not appear to cover the entire germ cell, as revealed by high-power views. Nevertheless there is sheath cell cytoplasm between these unsheathed germ cells (arrows) that may reflect filopodia extending between them (see Fig. 5C). The germ cells are larger in C than in B because a younger animal (late L4/young adult) was analyzed and a more proximal plane of section was taken in C. There is no evidence for yolk uptake in these immature germ cells. Scale bar corresponds to 1.0 μm in A, 0.5 μm in the inset, and 5 μm in B and C.

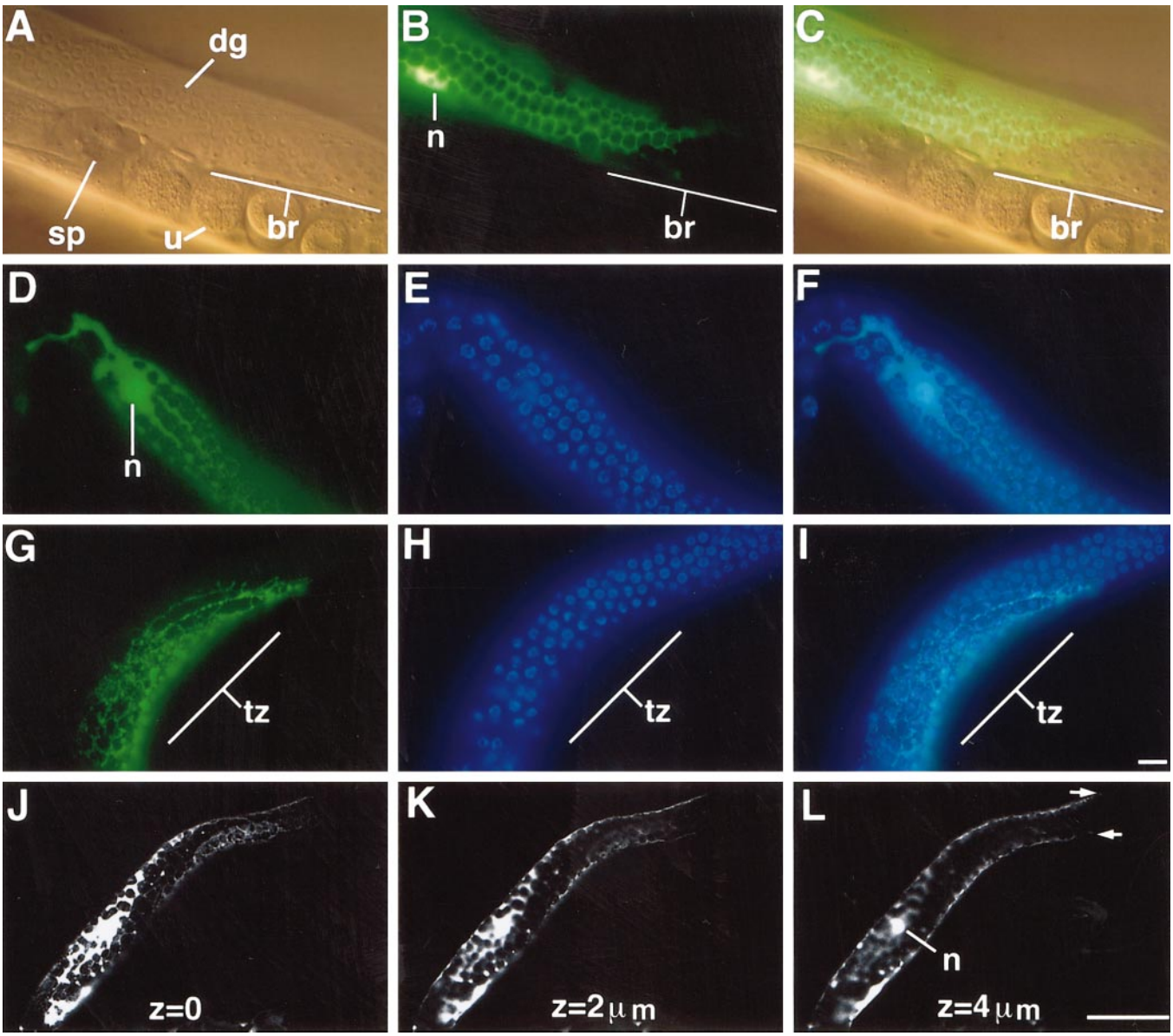

FIG. 10. Visualization of distal sheath cells. Pair 1 sheath cells were visualized using a GFP reporter construct (see Materials and Methods). (A–C) Visualization of distal sheath cells in a living animal. (A) Nomarski image focusing on germline nuclei in the distal arm of the gonad (dg). The spermatheca (sp) and the uterus (u) are indicated. (B) GFP fluorescence is seen as a honeycomb pattern in which the sheath cell cytoplasm is concentrated between germ cells. GFP fluorescence is limited to a superficial plane of focus corresponding to the gonad surface. The nucleus of sheath 1 is visible (n) with GFP excluded from its prominent nucleolus. (C) Merged Nomarski and fluorescence images. The bare region in the distal arm is indicated (br). (D–L) Visualization of distal sheath cells in dissected gonadal preparations. GFP fluorescence (D, G), the respective DAPI images (E, H), and merged images (F, I), focusing on the proximal (D–F) and distal (G–I) margins of sheath cell 1, respectively. A lower plane of focus was chosen to visualize the germline nuclei. The sheath 1 soma projects proximally between germ cells reaching just past the loop (D, F). Distal projecting filopodia project between germ cells and reach just past the transition zone (tz) where nuclei undergo the transition from the mitotic cell cycle to meiotic prophase (G–I). (J–L) GFP fluorescence visualized using serial confocal z-series sections differing by 2 μm: (J) surface view, (L) interior view. The nucleus (n) of one sheath 1 cell is visible in L. The distal margins of the two sheath cells are indicated by arrows in L. This series emphasizes the thinness of the distal sheath, its incompleteness, and the concentration of the sheath cell cytoplasm between the germ cells. Distal is at the right in all panels. Scale bar for A–I is shown in I and corresponds to 10 μm. Scale bar for J–L is shown in L and corresponds to 50 μm.

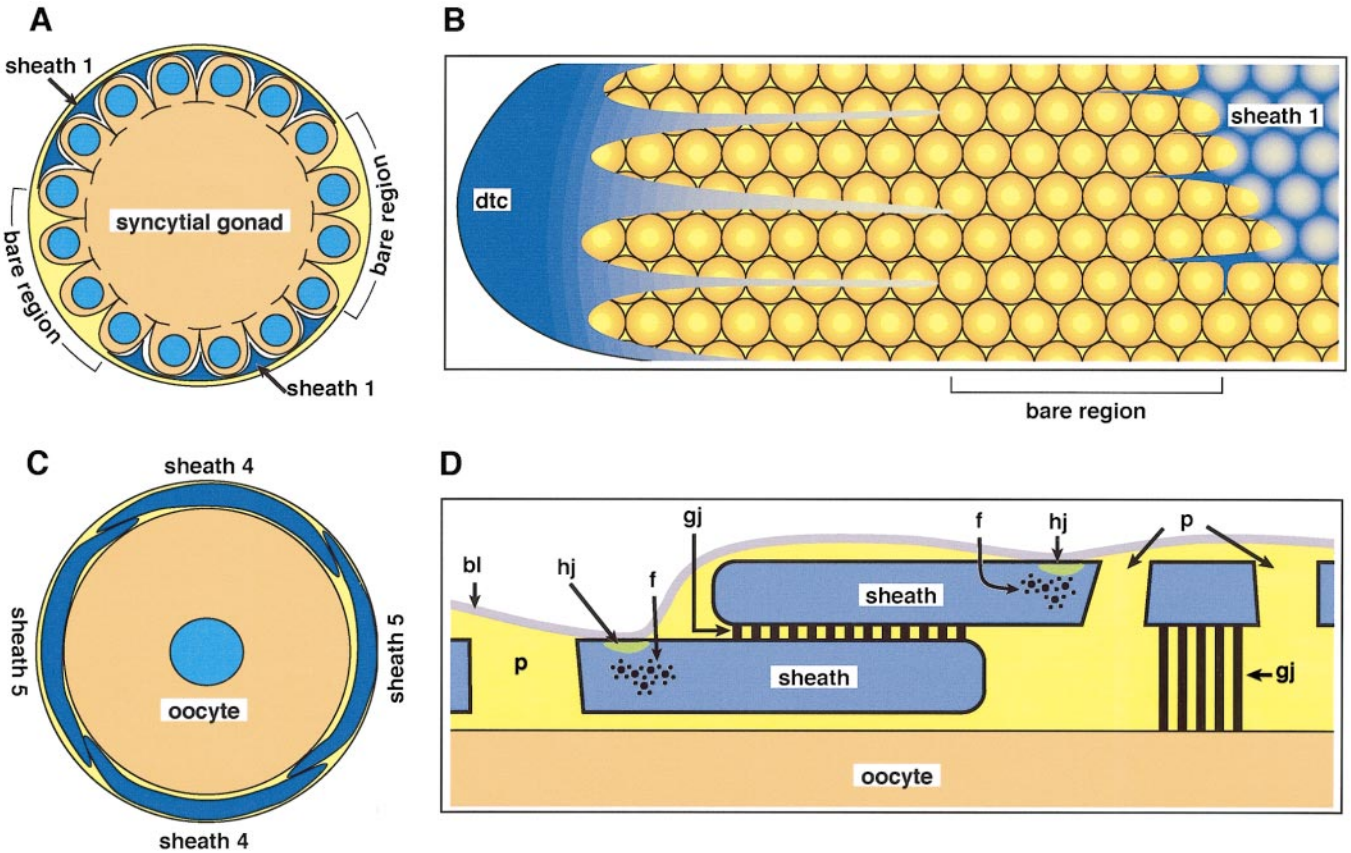

FIG. 11. Summary of ultrastructural features. Schematic representation of the distal (A, B) and proximal gonad (C, D). (A) Cross section of the distal arm from the proximal end of the transition zone showing the syncytial germ cell nuclei (light blue) connected to the core cytoplasm or rachis. Pair 1 sheath cells (dark blue) do not completely cover the gonad arm, resulting in bare regions where syncytial germ cells are covered only by the gonadal basal lamina. The cytoplasm of sheath cell 1 inserts between germ cells in a space-filling manner. (B) Representation of the distal arm in which the gonad has been cut along the distal–proximal axis and opened up. The dtc (at left) covers germ cells and extends processes proximally. Sheath cell 1 (at right) extends filopodia distally. There is a bare region between the dtc and sheath cell 1. The precise length and arrangement of the bare regions seem to be variable. (C) Cross-section of the proximal arm from a region where sheath cell pair 4 meets sheath cell pair 5. Proximal sheath cells completely cover the proximal arm and are closely apposed to the oocyte beneath the gonadal basal lamina. The precise arrangement of proximal sheath cells at regions of overlap has not been determined. (D) Ultrastructural features of proximal sheath cells and oocytes. Sheath/sheath and sheath/oocyte gap junctions are observed (gj). For illustrative purposes, short bars are used to denote sheath/sheath gap junctions and long bars are used to denote sheath/oocyte gap junctions. At the ultrastructural level, these gap junctions have a similar appearance; whether there are molecular differences in their composition is unknown. Sheath myofilaments (f) are anchored to hemi-adherens junctions (hj) which in turn are closely apposed to the basal lamina (bl). Sheath pores (p) permit the transit of yolk particles to oocytes.

Meiotic Maturation and Ovulation

During meiotic maturation, the oocyte enters meiotic M-phase from prophase and undergoes a structural change termed cortical rearrangement (Ward and Carrel, 1979; McCarter *et al.*, 1999). These germline events coincide with a reproducible sequence of somatic motor events, involving the proximal myoepithelial gonadal sheath cells and the distal spermatheca, that lead to the ovulation and fertilization of the mature oocyte. Proximal sheath cell pairs 3–5 form a thin layer between the gonadal basal lamina and the oocytes (see Figs. 1 and 2A). Pair 5 sheath cells directly attach to the distal spermatheca (D. Hall, L. P. Winfrey, L. H. Hoffman, and D. Greenstein, unpublished results). As nuclear envelope breakdown approaches (~5 min prior to ovulation), the contractions of the proximal sheath cells increase in frequency and intensity (McCarter *et al.*, 1999; Rose *et al.*, 1997). During ovulation, the proximal sheath cells pull the dilating distal spermatheca over the mature oocyte. The oocyte is rapidly fertilized as it comes into contact with activated sperm located in the spermatheca (Ward and Carrel, 1979). This sequence of events is faithfully executed with a periodicity of approximately 20–50 min, such that each gonad arm of an adult hermaphrodite produces approximately 160 self-progeny in 3 days (Hirsh *et al.*, 1976).

Previous results have suggested that coupling between meiotic maturation and ovulation may be essential for fertilization (Iwasaki *et al.*, 1996; McCarter *et al.*, 1997; Rose *et al.*, 1997). Mature oocytes that are not ovulated on schedule become endomitotic within the gonad arm and never undergo embryogenesis if they are ovulated at a later time (Iwasaki *et al.*, 1996; Myers *et al.*, 1996; McCarter *et al.*, 1997; Rose *et al.*, 1997). Similarly, when immature oocytes are ovulated, embryonic development does not occur (Rose *et al.*, 1997). How are germline and somatic events reproducibly coordinated to ensure production of the maximum number of viable diploid zygotes? Recently, McCarter *et al.* (1999) have shown that a sperm-associated signal(s) promotes oocyte meiotic maturation and stimulates sheath contraction. In turn, the maturing oocyte modulates sheath contractions at ovulation and induces spermathecal dilation (McCarter *et al.*, 1999) using a *let-23* signal transduction pathway (J. McCarter, B. Bartlett, T. Dang, R. Hill, M. Lee, and T. Schedl, unpublished results) involving the *lfe-1* and *lfe-2* genes (Clandinin *et al.*, 1998). We have observed sheath/oocyte gap junctions by two independent electron microscopic methods: (1) thin-section TEM analysis of intact and dissected gonadal preparations and (2) freeze-fracture analysis. The existence of sheath/oocyte gap junctions provides a potential mechanism whereby electrical or molecular signals passing between sheath and oocyte could coordinate their behaviors. The possibility that sheath cells may modulate maturation positively is consistent with the findings that sheath cell ablations and *ceh-18* mutations result in delays in oocyte meiotic maturation (McCarter *et al.*, 1997; Rose *et al.*, 1997). In *ceh-18(mg57)* mutants, sheath cells are less closely apposed to oocytes and sheath/oocyte gap junctions are rare or absent (Rose *et al.*, 1997; data not shown). McCarter *et al.* (1999) provided evidence that direct contact between oocytes and the most proximal sheath cells (pairs 4 and 5) is not necessary for oocyte maturation. Thus, we expect that sheath/oocyte gap junctions are not required for oocyte maturation per se, but could have a modulatory role. We speculate that communication through these junctions may modulate or coordinate meiotic maturation and sheath motility. Likewise, sheath/sheath gap junctions may serve to electrically couple proximal sheath cells to achieve the coordinated series of contractions necessary to ovulate the mature oocyte.

Sheath/oocyte junctions must be dynamic since individual oocytes lose contact with sheath cells when they are ovulated. At present, there are no data as to what molecules cross these junctions or the direction in which they pass. Attempts to visualize communication across these junctions using physiological dye injections (e.g., lucifer yellow) have been problematic due to difficulties in resolving the thin sheath cell bodies *in vivo* (D. Greenstein, unpublished results). In mammals, gap junctions exist between the oocyte and ovarian cumulus cells (Anderson and Albertini, 1976). Transport of cAMP through these junctions has been proposed to regulate meiotic maturation of the oocyte (for review see Wickramsinghe and Albertini, 1993). Targeted disruption of the connexin 37 gene in the mouse causes defects in oogenesis and ovulation (Simon *et al.*, 1997), supporting the idea that communication through oocyte/cumulus cell gap junctions is essential.

Recently, Starich *et al.* (1996) have proposed that the innexin gene family, defined by the *Drosophila l(1)ogre* and *shaking-B* (also called *passover*) genes and the *C. elegans unc-7* and *eat-5* genes, is required for the formation of invertebrate gap junctions (see also Finbow, 1997). According to this hypothesis, innexins may represent invertebrate versions of the connexins that form gap junctional channels in vertebrates, although there is no sequence similarity between the vertebrate and invertebrate genes. Despite this lack of sequence similarity, both innexins and connexins are proposed to share a similar structure with four transmembrane domains separating two extracellular loops and one cytoplasmic loop (Goodenough *et al.*, 1996; Phelen *et al.*, 1998a). Strong support for this hypothesis comes from the finding that the *Drosophila* Shaking-B protein forms gap junctions in paired *Xenopus* oocytes (Phelen *et al.*, 1998b). Currently, about 24 genes are believed to comprise this innexin gene family in *C. elegans* (Barnes and Hekimi, 1997; Phelen *et al.*, 1998a). An antibody against one of the *C. elegans* innexins labels gap junctions in the pharynx and in early embryos by immunoEM (D. Hall, T. Starich, A. Miller, and J. Shaw, unpublished results). It will be interesting to determine which members are expressed in sheath cells and oocytes and contribute to the formation of these singularly large gap junctions. Ultimately, mutational analysis of sheath/oocyte gap junctional components will be required to establish their *in vivo* function.

In order for myofilament contractions to alter sheath cell shape, the myofilaments must be anchored to the plasma membrane and the basal lamina to enable the transmission of tensile forces. Our results suggest that hemi-adherens junctions serve to anchor the contractile apparatus in sheath cells. Thin filaments are closely associated with these electron-dense plaque-like structures and appear, on favorable views, to project obliquely into them. In addition, the hemi-adherens junctions serve as attachment points for the gonadal basal lamina. Similar hemi-adherens junctions anchor the myofilaments to the plasma membrane and to the basal lamina in pharyngeal muscle cells (previously termed "half desmosomes" by Albertson and Thomson, 1976). Sheath cell hemi-adherens junctions also resemble the membrane-associated dense bodies of vertebrate smooth muscle cells (Chou *et al.*, 1992), further supporting the notion that the proximal gonadal sheath cells are myoepithelial smooth muscle-like cells (Strome, 1986; McCarter *et al.*, 1997; Rose *et al.*, 1997).

In *C. elegans* body wall muscle cells, actin filaments are anchored at larger more elaborate structures termed dense bodies that project from the sarcolemma into the muscle cell cytoplasm and organize the sarcomeres (Francis and Waterston, 1985). Several observations suggest that sheath hemi-adherens junctions share some components in com-

mon with body wall muscle dense bodies. First, sheath cells express a number of muscle dense body components including a functional *pat-2* α integrin–*gfp* fusion (B. Williams, personal communication), *unc-52* perlecan (K. Rose and D. Greenstein, unpublished results), and *pat-3* β integrin (Gettner *et al.*, 1995; K. Rose and D. Greenstein, unpublished results). These markers display a "dot-like" staining pattern that localizes to the basal surface of the proximal sheath cells. Second, mutations in *unc-52* and an interacting gene, *sup-38*, cause gonadal defects (Gilchrist and Moermann, 1992; Rogalski *et al.*, 1993, 1995). Third, mutations in *pat-3* (formerly called *epi-2*) and in *epi-1* (encodes laminin αB) cause defects in gonad sheath epithelialization, as well as body wall muscle defects, apparently due to poor muscle–lamina attachments in both tissues (D. Hall, W. G. Wadsworth, and E. Hedgecock, unpublished observations; Gettner *et al.*, 1995). Finally, *unc-52(e998)* mutants exhibit an unusual phenotype when sheath cell contractions are observed by time-lapse Nomarski videomicroscopy: the sheath cells appear to slide with respect to the gonadal basal lamina when they contract, suggesting that adherence between the sheath cells and the basal lamina is compromised (D. Greenstein, unpublished observations).

A Model for Yolk Transport into Oocytes

Electron microscopic analysis has revealed that the proximal sheath cells have a novel structure with multiple small pores forming conduits through the sheath cell to the surface of the oocyte. Sheath pores were observed by three independent EM methods: (1) thin-section analysis of intact and dissected gonadal preparations, including serial-section analysis of intact animals; (2) freeze-fracture analysis; and (3) SEM analysis. Thin sections and immunoEM of intact animals suggested that yolk protein particles were associated with the sheath pores. Previously, Doniach and Hodgkin (1984) used TEM to compare the appearance of oocytes from the wild type with those found in a sex determination mutant combination that produces oocytes but no yolk proteins. Based on this analysis it was suggested that the electron-dense granules within the oocyte were yolk granules. Our immunoEM results support this hypothesis.

Based on these results, we propose that yolk particles pass through the gonadal basal lamina, move through sheath pores, and are endocytosed by oocytes. We found little evidence for transcytosis of yolk particles through sheath cells by electron microscopy, immunofluorescence, or immunoEM. Yolk uptake is highly asymmetric and most frequently occurs in the three most proximal oocytes in young adults. Yolk uptake by fertile adult hermaphrodites appears to be a highly efficient process: most yolk is observed within the intestine or entering oocytes; almost none is seen within sheath cells, and very little is seen in the pseudocoelom. These observations lead us to speculate that yolk transfer through sheath pores is an active process. Furthermore, mutations which interfere with oocyte formation or development cause a buildup of yolk in the pseudocoelom but not in sheath cells, suggesting that demand for more yolk by proximal oocytes drives an active process that is unlikely to involve transcytosis (D. Hall and D. Greenstein, unpublished results). If yolk was transported to oocytes via sheath cell transcytosis, we would expect that yolk would accumulate in proximal sheath cells in oocyte development mutants.

Yolk uptake by proximal oocytes shows structural hallmarks of endocytosis: membrane specialization is observed on the cytoplasmic side of the oocyte membrane where apposed to yolk particles (i.e., the contact point) and this membrane deforms to create characteristic out-pocketings. This observation was contrary to our expectation that in-pocketings would be more common at these contact points. One possibility is that the characteristic membrane out-pocketings represent an early intermediate in yolk uptake.

The sheath pores are unusual cellular structures and the mechanism by which they are assembled or stabilized is unknown. Similar cellular structures are found in vertebrate endothelial cells that comprise fenestrated capillaries. Although endothelial cell fenestrae in many organs are covered by thin diaphragms, the 60- to 80-nm-diameter pores in mammalian glomerular capillary endothelium are open, similar to the pores in *C. elegans* sheath cells. Open fenestrae of sinusoidal endothelia in liver are even less regular in shape and reach diameters of several hundred nanometers (Simionescu and Simionescu, 1988). Endothelial cell pores facilitate selective permeability required for efficient absorption, secretion, and filtering (see Cines *et al.*, 1998, for a review) in a similar fashion to which sheath pores facilitate yolk transport. We speculate that there are similarities in the developmental mechanisms by which pores form in these vastly different cell types. It is not known how yolk particles are able to pass through the gonadal basal lamina. It is also unclear whether sheath pores change in size when the sheath cell contracts; however, SEM data show that pores can be stretched by artifactual forces arising during the preparation of the sample. Recently, Fire *et al.* (1998) have shown that double-stranded RNA-mediated gene interference can be observed in the germ line following injections into the pseudocoelom or the intestine. We speculate that the injected RNA enters the germ line in part through sheath pores.

The Role of Distal Sheath Cells

Recently, McCarter *et al.* (1997) reported an extensive series of cell ablation experiments demonstrating that cells of the sheath-spermathecal (SS) lineages promote germline proliferation and pachytene exit. Specifically, the distal sheath cells (pairs 1 and 2) were suggested to promote pachytene exit. In young adults, germ cells exit the pachytene stage of meiosis as they traverse the gonad loop. Genetic analysis has demonstrated that genes of the RAS and MAP kinase pathways are also required in the germ line for pachytene exit (Church *et al.*, 1995). A major phenotypic difference is that mutations in RAS/MAP kinase pathway

genes also result in germ cell disorganization. An attractive hypothesis is that the distal sheath cells directly signal germ cells to exit the pachytene stage of the cell cycle using extracellular signaling molecules that trigger genes of the RAS MAP kinase pathway subsequent to receptor activation in the germ line. The identification of genes required in distal sheath cells for pachytene exit would provide strong support for this hypothesis.

The possibility that distal sheath cells provide nutritional support for germ cells was also considered (McCarter *et al.*, 1997). Our observations of close apposition of distal sheath cell processes and germ cells as well as the presence of rare adhesive junctions are suggestive of direct cell–cell interactions. The distal sheath cells are enriched in Golgi apparatus leading us to suggest that these cells may also have a secretory function. This hypothesized secretory function would fit well with the idea that distal sheath cells provide nutritional support for germ cells or provide growth factors to promote meiotic cell cycle progression. Development of distal germ cells is clearly not nourished by yolk protein, which is not found in distal germ cells or the rachis.

The Distal Tip Cell, Distal Sheath Cells, and the Mitotic Zone

The dtc regulates germ cell mitosis and entry into meiotic prophase (Kimble and White, 1981). According to the current model, the dtc expresses the LAG-2 ligand, which activates the GLP-1 Notch-family receptor in the germ line (Austin and Kimble, 1989; Lambie and Kimble, 1991; Crittenden *et al.*, 1994; Henderson *et al.*, 1994; Tax *et al.*, 1994). *glp-1* signaling in the germ line is necessary and sufficient to trigger entry into mitosis and/or inhibit entry into the meiotic pathway (Austin and Kimble, 1989; Berry *et al.*, 1997; Kadyk and Kimble, 1998). Signaling from Notch-family receptors has been extensively studied (see Artavanis-Tsakonas *et al.*, 1999, for a review) and several models have been presented for the inductive interaction mediated by GLP-1 (Yochem and Greenwald, 1989; Crittenden *et al.*, 1994; Henderson *et al.*, 1997). In *Drosophila*, analysis of genetic mosaics suggests that the Notch ligand Delta acts over a short range to signal adjacent cells (Heitzler and Simpson, 1991). Consistent with this observation, mutant analysis and transgenic experiments revealed a critical role of the transmembrane domain for LAG-2 function (Henderson *et al.*, 1997). Transgenic experiments also showed that truncated diffusible ligands could confer wild-type function, but abnormal development often ensued, owing to ectopic proliferation (Fitzgerald and Greenwald, 1995; Henderson *et al.*, 1997). Thus, the extent to which the dtc contacts germ cells is likely to be a critical parameter for understanding the inductive interaction in the wild-type gonad. We have visualized the dtc processes using SEM, TEM, and fluorescence microscopy. The dtc processes make close contact with germ cells in the mitotic zone. Both SEM and TEM analyses show that the dtc processes are continuous with the cell body. The lengths of the dtc processes tend to vary, but they tend to be shorter than the maximal extent of the mitotic zone (average of 8 ± 4 germ cell diameters from the distal tip). The observation that germ cells located within approximately the first 10 cell diameters from the dtc are likely to be located within ~2 cell diameters of a dtc process suggests that as germ cells move proximally they may encounter a process. Similarly, new germ cells born in the mitotic zone may also contact a dtc process. It will be important to determine whether the dtc processes are dynamic by obtaining time-resolved images of the dtc processes *in vivo*. It is possible that the dtc signal may also be presented to germ cells in the form of secreted or shed dtc material. For example, other TEM data indicate that the dtc is vigorously secretory. In fact, fragments of detached or shed dtc material were frequently observed trailing beyond the dtc processes by TEM (D. Hall and E. Hedgecock, unpublished results). Such shed dtc material may retain biological activity.

Direct visualization of pair 1 sheath cells using a GFP reporter established that these cells extend over the distal arm to reach approximately 19 germ cell diameters from the distal tip cell. Thus, the distal extent of pair 1 sheath cells correlates with the proximal border of the mitotic zone (Crittenden *et al.*, 1994). We speculate that the distal sheath cells may restrict the diffusion of the LAG-2 ligand from the dtc (Henderson *et al.*, 1994), thereby contributing to the sharp border of the mitotic zone (Crittenden *et al.*, 1994). Consistent with this hypothesis, mutations in *epi-1* result in detachment of the distal sheath cells from the germ line and also cause germ cell overproliferation (D. Hall and E. Hedgecock, unpublished data). Despite these consistent data, further experiments will be needed to determine whether the distal sheath cells regulate germ cell mitosis. If this speculation is borne out by subsequent experimentation, then it is likely that cells of the sheath-spermathecal lineages can have both positive and negative effects on germline proliferation because McCarter *et al.* (1997) demonstrated that ablation of both SS cells in a gonad arm results in defective germline proliferation.

Germ cells divide distally and move proximally as they enter meiosis and undergo gametogenesis. How does the distal sheath maintain its position relative to a moving germ line? One possibility is that the distal sheath's longitudinal cytoskeletal elements and filopodia function to retain the sheath's "grip" upon the outer edge of the germ cells, in effect pulling the sheath past the germ cells as they slowly move proximally underneath. Although formally possible, the intricate cytoskeletal reinforcements underlying the distal sheath's insertion between germ cells, the presence of focal adhesions, and the very delicate nature of the thinner portions of the sheath argue against this possibility. Alternatively, sheath cell 1 could grow distally at roughly the same rate as the mitotic germ line creates new unsheathed germ cells in the bare region with new sheath membrane being added distally (cf. Pfenninger and Friedman, 1993) and older membrane recycled at some proximal locale. According to this model, the distal sheath filopodia

may actively search in a distal direction in order to extend and grow new sheath elements to cover the bare region. Without such action, the distal border of sheath cell 1 might gradually drift proximally, leaving more germ cells exposed. Studies of mutants as well as experimental manipulations of living gonads may help to resolve these possibilities.

ACKNOWLEDGMENTS

This paper is dedicated to the memory of Dr. Loren H. Hoffman, a wonderful cell biologist, teacher, and friend. We thank Peg MacMorris and Barth Grant for antibodies to yolk proteins. We thank Barth Grant for providing the *vit-2::gfp* strain and Marie-Christine Paupard and Agness Miller for help with immunoEM. We thank Iva Greenwald and Tim Schedl for providing the *lag-2::gfp* strain and helpful discussions. Ed Hedgecock, Todd Starich, Jocelyn Shaw, Bill Wadsworth, and Ben Williams generously shared unpublished data. The authors are grateful to Jane Hubbard, Jay Kirchner, David Miller, and Chris Wright for helpful discussions and comments on the manuscript. We thank the two anonymous reviewers for providing helpful comments. This work was supported by grants from the American Cancer Society (DB-149 and JFRA-630) and the National Institutes of Health (GM57173) to D.G. The Center for *C. elegans* Anatomy is supported by NIH RR12596 to D.H.H. Core facilities for electron microscopy were provided through NIH Center Grant HD05797 to L.H.H. Laser-scanning confocal microscopy was performed at the VUMC Cell Imaging Resource Center (supported by CA68485 and DK20593) with the help of Jonathan Sheehan. Some strains used in this study were provided by the *Caenorhabditis* Genetics Center which is supported by the National Institutes of Health's National Center for Research Resources.

REFERENCES

Abi-Rached, M., and Brun, J. L. (1975). 'Etude ultrastructurale des relations entre ovocytes et rachis au cours de l'ovogenese du nematode *C. elegans. Nematologica* **21,** 151–162.

Albertson, D. G., and Thomson, J. N. (1976). The pharynx of *Caenorhabditis elegans. Philos. Trans. Royal Soc.* **275B,** 299–325.

Anderson, E., and Albertini, D. F. (1976). Gap junctions between the oocyte and companion follicle cells in mammalian ovary. *J. Cell Biol.* **71,** 680–686.

Artavanis-Tsakonas, S., Rand, M. D., and Lake, R. J. (1999). Notch signaling: Cell fate control and signal integration in development. *Science* **284,** 770–776.

Austin, J., and Kimble, J. (1987). *glp-1* is required in the germ line for regulation of the decision between mitosis and meiosis in *C. elegans. Cell* **51,** 589–599.

Barnes, T. M., and Hekimi, S. (1997). The *Caenorhabditis elegans* avermectin resistance and anesthetic response gene *unc-9* encodes a member of a protein family implicated in electrical coupling of excitable cells. *J. Neurochem.* **69,** 2251–2260.

Berry, L. W., Westlund, B., and Schedl, T. (1997). Germ-line tumor formation caused by activation of *glp-1*, a *Caenorhabditis elegans* member of the Notch family of receptors. *Development* **124,** 925–936.

Buechner, M., Hall, D. H., Bhatt, H., and Hedgecock, E. M. (1999). Cystic canal mutants in *C. elegans* are defective in the apical membrane domain of the renal (excretory) cell. Submitted.

Chou, R. G., Stromer, M. H., Robson, R. M., and Huiatt, T. W. (1992). Assembly of contractile and cytoskeletal elements in developing smooth muscle cells. *Dev. Biol.* **149,** 339–348.

Church, D. L., Guan, K.-L., and Lambie, E. J. (1995). Three genes of the MAP kinase cascade, *mek-2, mpk-1*/*sur-1* and *let-60 ras,* are required for meiotic cell cycle progression in *Caenorhabditis elegans. Development* **121,** 2525–2535.

Cines, D. B., Pollak E. S., Buck, C. A., Loscalzo, J., Zimmerman, G. A., McEver, R. P., Pober, J. S., Wick, T. M., Konkle, B. A., Schwartz, B. S., Barnathan, E. S., McCrae, K. R., Hug, B. A., Schmidt, A.-M., and Stern, D. M. (1998). Endothelial cells in physiology and in the pathophysiology of vascular disorders. *Blood* **91,** 3527–3661.

Clandinin, T. R., DeModena, J. A., and Sternberg, P. W. (1998). Inositol triphosphate mediates a RAS-independent response to LET-23 receptor tyrosine kinase activation in *C. elegans. Cell* **92,** 523–533.

Crittenden, S. L., Troeml, E. R., Evans, T. C., and Kimble, J. (1994). GLP-1 is localized to the mitotic region of the *C. elegans* germ line. *Development* **120,** 2901–2911.

Dolci, S., Williams, D. E., Ernst, M. K., Resnick, J. L., Braman, C. I., Fock, L. F., Lyman, S. D., Boswell, S. H., and Donovan, P. J. (1991). Requirements for mast cell growth factor for primordial germ cell survival in culture. *Nature* **352,** 809–811.

Dolci, S., Pesce, M., and De Felici, M. (1993). Combined action of stem cell factor, leukemia inhibitory factor, and cAMP on *in vitro* proliferation of mouse primordial germ cells. *Mol. Reprod. Dev.* **35,** 134–139.

Doniach, T., and Hodgkin, J. (1984). A sex-determining gene, *fem-1,* required for both male and hermaphrodite development in *Caenorhabditis elegans. Dev. Biol.* **106,** 223–235.

Finbow, M. E. (1997). Vetebrate and invertebrate gap junctions: A common molecular basis? *Cell Biol. Int.* **21,** 329–331.

Fire, A., Xu, S., Montgomery, M. K., Kostas, S. A., Driver, S. E., and Mello, C. C. (1998). Potent and specific genetic interference by double-stranded RNA in *Caenorhabditis elegans. Nature* **391,** 806–811.

Fitzgerald, K., Wilkinson, H., and Greenwald, I. (1993). *glp-1* can substitute for *lin-12* in specifying cell fate decisions in *C. elegans. Development* **119,** 1019–1027.

Fitzgerald, K., and Greenwald, I. (1995). Interchangeability of *Caenorhabditis elegans* DSL proteins and intrinsic signalling activity of their extracellular domains *in vivo. Development* **121,** 4275–4282.

Fleischman, R. A. (1993). From white spots to stem cells: The role of the Kit receptor in mammalian development. *Trends Genet.* **9,** 285–290.

Francis, G. R., and Waterston, R. H. (1985). Muscle organization in *Caenorhabditis elegans:* Localization of proteins implicated in thin filament attachment and I-band organization. *J. Cell Biol.* **101,** 1532–1549.

Francis, R., Barton, M. K., Kimble, J., and Schedl, T. (1995). *gld-1,* a tumor suppressor gene required for oocyte development in *Caenorhabditis elegans. Genetics* **139,** 579–606.

Gettner, S. N., Kenyon, D., and Reichardt, L. F. (1995). Characterization of beta-pat-3 heterodimers, a family of essential integrin receptors in *C. elegans. J. Cell Biol.* **129,** 1127–1141.

Gilchrist, E. J., and Moerman, D. G. (1992). Mutations in the *sup-38* gene of *Caenorhabditis elegans* suppress muscle-attachment defects in *unc-52* mutants. *Genetics* **132,** 431–442.

Goodenough, D. A., Goliger, J. A., and Paul, D. L. (1996). Connexins, connexons, and intercellular communication. *Annu. Rev. Biochem.* **65,** 475–502.

Greenstein, D., Hird, S., Plasterk, R. H. A., Andachi, Y., Kohara, Y., Wang, B., Finney, M., and Ruvkun, G. (1994). Targeted mutations in the *Caenorhabditis elegans* POU homeobox gene *ceh-18* cause defects in oocyte cell cycle arrest, gonad migration, and epidermal differentiation. *Genes Dev.* **8,** 1935–1948.

Hall, D. H. (1987). Freeze fracture and freeze etch studies of the nematode, *Caenorhabditis elegans. Ann. N. Y. Acad. Sci.* **494,** 215–217.

Hall, D. (1995). Electron microscopy and three-dimensional image reconstruction. In "*Caenorhabditis elegans:* Modern Biological Analysis of an Organism, Methods in Cell Biology" (H. F. Epstein and D. C. Shakes, Eds.), Vol. 48, pp. 395–436. Academic Press, San Diego.

Heitzler, P., and Simpson, P. (1991). The choice of cell fate in the epidermis of *Drosophila. Cell* **64,** 1083–1092.

Henderson, S. T., Gao, D., Lambie, E. J., and Kimble, J. (1994). *lag-2* may encode a signaling ligand for the GLP-1 and LIN-12 receptors of *C. elegans. Development* **120,** 2913–2924.

Henderson, S. T., Gao, D., Christensen, S., and Kimble, J. (1997). Functional domains of LAG-2, a putative signaling ligand for LIN-12 and GLP-1 receptors in *Caenorhabditis elegans. Mol. Biol. Cell* **8,** 1751–1762.

Hirsh, D., Oppenheim, D., and Klass, M. (1976). Development of the reproductive system of *Caenorhabditis elegans. Dev. Biol.* **49,** 200–219.

Iwasaki, K., McCarter, J., Francis, R., and Schedl, T. (1996). *emo-1,* a *Caenorhabditis elegans* Sec61p gamma homologue, is required for oocyte development and ovulation. *J. Cell Biol.* **134,** 699–714.

Kadyk, L. C., and Kimble, J. (1998). Genetic regulation of entry into meiosis in *Caenorhabditis elegans. Development* **125,** 1803–1813.

Keshet, E., Lyman, S. D., Williams, D. E., Anderson, D. M., Jenkins, N. A., Copeland, N. G., and Parada, L. F. (1991). Embryonic RNA expression patterns of the c-kit receptor and its cognate ligand suggest multiple functional roles in mouse development. *EMBO J.* **10,** 2425–2435.

Kimble, J., and Hirsh, D. (1979). The postembryonic cell lineages of the hermaphrodite and male gonads in *Caenorhabditis elegans. Dev. Biol.* **70,** 396–417.

Kimble, J., and Sharrock, W. J. (1983). Tissue-specific synthesis of yolk proteins in *Caenorhabditis elegans. Dev. Biol.* **96,** 189–196.

Kimble, J., and White, J. (1981). On the control of germ cell development in *Caenorhabditis elegans. Dev. Biol.* **81,** 208–219.

Kramer, J., French, R. P., Park, E., and Johnson, J. J. (1990). The *Caenorhabditis elegans rol-6* gene, which interacts with the *sqt-1* collagen gene to determine organismal morphology, encodes a collagen. *Mol. Cell Biol.* **10,** 2081–2090.

Lambie, E. J., and Kimble, J. (1991). Two homologous regulatory genes, *lin-12* and *glp-1,* have overlapping functions. *Development* **112,** 231–240.

Lane, N. J., and Flores, V. (1990). The role of cytoskeletal components in the maintenance of intercellular junctions in an insect. *Cell Tissue Res.* **262,** 373–385.

L'Hernault, S. W. (1997). Spermatogenesis. In "*C. elegans* II" (D. L. Riddle, T. Blumenthal, B. J. Meyer, and J. R. Priess, Eds.). Cold Spring Harbor Laboratory Press, Cold Spring Harbor, NY.

Marziali, B., Lazzaro, D., and Sorrentino, V. (1993). Binding of germ cells to mutant Sld Sertoli cells is defective and is rescued by expression of the transmembrane form of the c-kit ligand. *Dev. Biol.* **157,** 182–190.

Matsui, Y., Zsebo, K. M., and Hogan, B. L. M. (1990). Embryonic expression of a haematopoietic growth factor encoded by the Sl locus and the ligand for c-kit. *Nature* **347,** 666–669.

McCarter, J., Bartlett, B., Dang, T., and Schedl, T. (1997). Soma–germ cell interactions in *Caenorhabditis elegans:* Multiple events in germline development require the somatic sheath and spermathecal lineages. *Dev. Biol.* **181,** 121–143.

McCarter, J., Bartlett, B., Dang, T., and Schedl, T. (1999). On the control of oocyte meiotic maturation and ovulation in *C. elegans. Dev. Biol.* **205,** 111–128.

Mello, C., and Fire, A. (1995). DNA transformation. In "*Caenorhabditis elegans:* Modern Biological Analysis of an Organism, Methods in Cell Biology" (H. F. Epstein and D. C. Shakes, Eds.), Vol. 48, pp. 395–436. Academic Press, San Diego.

Moerman, D. G., and Fire, A. (1997). Muscle: Structure, function, and development. In "*C. elegans* II" (D. L. Riddle, T. Blumenthal, B. J. Meyer, and J. R. Priess, Eds.). Cold Spring Harbor Laboratory Press, Cold Spring Harbor, NY.

Mukherjee, S., Ghosh, R. N., and Maxfield, F. R. (1997). Endocytosis. *Physiol. Rev.* **77,** 759–803.

Myers, C. D., Goh, P.-Y., Allen, T. StC., Bucher, E. A., and Bogaert, T. (1996). Developmental genetic analysis of Troponin T mutations in striated and nonstriated muscle cells of *Caenorhabditis elegans. J. Cell Biol.* **132,** 1061–1077.

Nagato, T., Yoshida, H., Yoshida, A., and Uehara, Y. (1980). A scanning electron microscope study of myoepithelial cells in exocrine glands. *Cell Tissue Res.* **209,** 1–10.

Newman, A. P., White, J. G., and Sternberg, P. W. (1996). Morphogenesis of the *C. elegans* hermaphrodite uterus. *Development* **122,** 3617–3626.

Pesce, M., Di Carlo, A., and De Felici, M. (1997). The c-kit receptor is involved in the adhesion of mouse primordial germ cells to somatic cells in culture. *Mech. Dev.* **68,** 37–44.

Pfenninger, K. H., and Friedman, L. B. (1993). Sites of plasmalemmal expansion in growth cones. *Dev. Brain Res.* **71,** 181–192.

Phelan, P., Bacon, J. P., Davies, J. A., Stebbings, L. A., Todman, M., Avery, L., Baines, R. A., Barnes, T. M., Ford, C., Hekimi, S., Lee, R., Shaw, J. E., Starich, T. A., Curtin, K. D., Sun, Y., and Wyman, R. J. (1998a). Innexins: A family of invertebrate gap-junction proteins. *Trends Genet.* **14,** 348–349.

Phelan, P., Stebbings, L. A., Baines, R. A., Bacon, J. P., Davies, J. A., and Ford, C. (1998b). *Drosophila* Shaking-B protein forms gap junctions in paired *Xenopus* oocytes. *Nature* **391,** 181–184.

Quick, D. C., and Johnson, R. G. (1977). Gap junctions and rhombic particle arrays in planaria. *J. Ultrastruct. Res.* **60,** 348–361.

Rogalski, T. M., Williams, B. D., Mullen, G. P., and Moerman, D. G. (1993). Products of the *unc-52* gene in *Caenorhabditis elegans* are homologous to the core protein of the mammalian basement membrane heparan sulfate proteoglycan. *Genes Dev.* **7,** 1471–1484.

Rogalski, T. M., Gilchrist, E. J., Mullen, G. P., and Moerman, D. G. (1995). Mutations in the *unc-52* gene responsible for body wall muscle defects in adult are located in alternatively spliced exons. *Genetics* **139,** 159–169.

Rose, K. L., Winfrey, V. P., Hoffman, L. H., Hall, D. H., Furuta, T., and Greenstein, D. (1997). The POU gene *ceh-18* promotes gonadal sheath cell differentiation and function required for meiotic maturation and ovulation in *Caenorhabditis elegans. Dev. Biol.* **192,** 59–77.

Schedl, T. (1997). Developmental genetics of the germ line. In "*C. elegans* II" (D. L. Riddle, T. Blumenthal, B. J. Meyer, and J. R. Priess, Eds.). Cold Spring Harbor Laboratory Press, Cold Spring Harbor, NY.

Sharrock, W. J. (1983). Yolk proteins of *C. elegans*. *Dev. Biol.* **96,** 182–188.

Sharrock, W. J. (1984). Cleavage of two yolk proteins from a precursor in *C. elegans*. *J. Mol. Biol.* **174,** 419–431.

Shen, M. M., and Hodgkin, J. (1988). *mab-3*, a gene required for sex-specific yolk protein expression and a male-specific lineage in *C. elegans*. *Cell* **54,** 1019–1031.

Simionescu, N., and Simionescu, M. The cardiovascular system. In "Cell and Tissue Biology" (L. Weiss, Ed.), 6th ed., pp. 353–400. Urban and Schwrzenberg, Baltimore, MD.

Simon, A. M., Goodenough, D. A., Li, E., and Paul, D. L. (1997). Female infertility in mice lacking connexin 37. *Nature* **385,** 525–529.

Simon, A. M., and Goodenough, D. A. (1998). Diverse functions of vertebrate gap junctions. *Trends Cell Biol.* **8,** 477–483.

Starich, T. A., Lee, R. Y. N., Panzarella, C., Avery, L., and Shaw, J. E. (1996). *eat-5* and *unc-7* represent a multigene family in *Caenorhabditis elegans* involved in cell–cell coupling. *J. Cell Biol.* **134,** 537–548.

Strome, S. (1986). Fluorescence visualization of the distribution of microfilaments in gonads and early embryos of the nematode *C. elegans*. *J. Cell Biol.* **103,** 2241–2252.

Tax, F. E., Yeargers, J. J., and Thomas, J. H. (1994). Sequence of *C. elegans lag-2* reveals a cell-signalling domain shared with Delta and Serrate of *Drosophila*. *Nature* **388,** 150–154.

Tepass, U., and Hartenstein, V. (1994). The development of cellular junctions in the *Drosophila* embryo. *Dev. Biol.* **161,** 563–596.

Ward, S., and Carrel, J. S. (1979). Fertilization and sperm competition in the nematode *Caenorhabditis elegans*. *Dev. Biol.* **73,** 304–321.

White, J. G. (1988). The anatomy. In "The Nematode *Caenorhabditis elegans*" (W. B. Wood, Ed.). Cold Spring Harbor Laboratory Press, Cold Spring Harbor, NY.

Wickramasinghe, D., and Albertini, D. F. (1993). Cell cycle control during mammalian oogenesis. *Curr. Top. Dev. Biol.* **28,** 125–153.

Yochem, J., and Greenwald, I. (1989). *glp-1* and *lin-12*, genes implicated in distinct cell–cell interactions in *C. elegans*, encode similar transmembrane proteins. *Cell* **58,** 553–563.

Received for publication March 9, 1999
Revised May 25, 1999
Accepted May 25, 1999